CONVECTIVE MIXING IN GEOLOGICAL CARBON STORAGE

PhD Thesis

MARIA ELENIUS

Department of Mathematics
University of Bergen

AUGUST 2011

Preface

This dissertation is submitted as a partial fulfillment of the requirements for the degree Doctor of Philosophy (PhD) at the University of Bergen. It is part of the project *Mathematical Modeling and Risk Assessment of CO_2 storage*, MatMoRA, which is funded by the Norwegian Research Council, Statoil and Norske Shell under grant no. 178013/I30 and lead by Professor Helge Dahle at the Department of Mathematics, University of Bergen (UiB). The working environment has been Uni Computing in Bergen. Research Director at Uni Computing, Klaus Johannsen, was the main adviser and Professor Jan M. Nordbotten at the Department of Mathematics, UiB, was co-adviser. Professor Hamdi A. Tchelepi at the Department of Energy Resources Engineering, Stanford University hosted the author during a six month research visit.

The objective of this thesis has been to contribute to the understanding of convective mixing in porous media, and especially on its influence on safe geological storage of carbon dioxide (CO_2). The interactions between the buoyant migration of supercritical CO_2 and the negatively buoyant fingering of dissolved CO_2 in geological formations is studied. Special focus is given to the capillary transition zone in this context. The time- and length-scales of convective mixing are studied in the linear as well as the nonlinear regime, using stability analysis and also statistical analysis based on multiple realizations of numerical simulations.

Outline

The thesis consists of two parts. The objective of Part I is to give a motivation and background to geological CO_2 storage and to introduce theory on multiphase flow and stability of miscible displacement. An overview of methods for direct numerical simulations is also presented. In addition, our results and conclusions are summarized and hypotheses and suggestions for future work are given, based on the collected results. A detailed description of our chosen methods, results and conclusions is presented in three articles which are included in Part II of the thesis:

Paper A: CO_2 trapping in sloping aquifers: High resolution numerical simulations. M.T. Elenius, H.A. Tchelepi and K. Johannsen. *Proceedings of XVIII International Conference on Water Resources*, 2010. Contribution of thesis author: implementation of of new initial condition procedure in the software GPRS, performance of simulations, analysis of results, writing the paper. Contribution of co-authors: ideas and suggestions for research and paper.

Paper B: Effects of a capillary transition zone on the stability of a diffusive boundary layer. M.T. Elenius, J.M. Nordbotten and H. Kalisch. Submitted to *IMA J. Appl. Math.* Contribution of thesis author: stability analysis, writing program for the full linear regime, performance of simulations for linear and nonlinear regime, writing the paper. Contribution of co-authors: ideas and suggestions for research and paper.

Paper C: On the time scales of non-linear instability in miscible displacement porous media flow. M.T. Elenius and K. Johannsen. Submitted to *Computational Geosciences*. Contribution of thesis author: performance of simulations, post-processing and analysis of results including error analysis, writing the paper. Contribution of co-author: performance of preliminary simulations, development of some of the pre- and post-processing tools, ideas and suggestions for research and paper.

Acknowledgements

After seven years of consulting, away from the University, I was very pleased to be given this chance to come back to the University, to learn more and to do interesting science.

Even before I moved to Bergen, my main adviser Research Director Klaus Johannsen gave helpful advice in a course I started taking at the University. That was a good start of a collaboration that I have enjoyed very much. Apart from the excellent knowledge Klaus has in porous media flow and on stability problems in particular, it has been very rewarding to work with someone who has such a joy and enthusiasm in solving problems, deriving equations and go into yet more detail of the numerics. Thank you Klaus! And thank you for the generosity with your time when I needed to talk with you.

My co-adviser Professor Jan Nordbotten has been very helpful and always invited me to the Knøderen sessions where he normally supervises his students. Jan has always been very focused and quick in getting to grips with my questions. He has a very good intuition on porous media flow and has inspired me a lot. Thank you Jan for all the good discussions! And thank you for caring and showing genuine interest in my research.

I am very thankful that I have been able to attend several conferences and given the opportunity to discuss my own and others work with colleagues around the world and on the weekly seminar series on flow in porous media and multi-scale methods. I have also had the pleasure of working with Professor Hamdi Tchelepi during a 6 month research visit at Stanford University. Thank you so much Hamdi for this invitation, for all the good discussions on gravity currents and stability

problems and for the numerous relevant literature suggestions! Thank you for hosting me so generously at Stanford.

Both in Bergen, at Stanford and other places I have been fortunate to find good collaboration partners also other than my advisers. I would especially like to thank Professor Helge Dahle for always caring about my research, Dr. Anozie Ebigbo for help with MUFTE when I was new, Dr. Denis Voskov and Dr. Yaqing Fan for help with GPRS, Professor Henrik Kalisch for the discussions regarding the stability paper, Group leader Eirik Thorsnes and his staff at Parallab for generous help on high-performance computing and related topics, Professor Rainer Helmig for sharing his limited time with great enthusiasm, Dr. Tomas Torsvik for having an open door for general discussions on analysis and numerics and Professor Ivar Aavatsmark for taking interest in my work from the very beginning. I am also so grateful to Ivar and CIPR for giving me the chance to continue doing research on CO_2 storage after my PhD!

Funding from the MatMoRA project and, during the last months the SUCCESS center, is greatly appreciated.

Thank you also all dear colleagues, for the shared laughs and thoughts. Especially thank you Kristin for all the walk-and-talks, this has meant a lot to me. Thank you Nicola for the tea-chats and also for proofreading the thesis introduction. I am very grateful to all my fun and caring friends and family in Bergen and elsewhere!

Abstract

The industrial era has seen an exponential growth in the atmospheric concentration of carbon dioxide (CO_2), resulting mainly from the burning of fossil fuels. This can cause changes in the climate that have severe impacts on freshwater and food supply, ecosystems and society. One of the most viable options to reduce CO_2 emissions is to store it in geological formations, in particular in saline aquifers. In this option, the carbon is again stored in the subsurface, from which it was extracted. The first geological storage project was initiated in Norway, in 1996, and CO_2 has long before been injected to geological formations to enhance oil recovery. Storage occurs with CO_2 in a so-called supercritical state and this fluid is buoyant in the formation. Four physical mechanisms help trapping the carbon in the formation: the CO_2 plume accumulates under a low-permeability caprock; CO_2 is trapped as disconnected drops in small pores; buoyancy is lost when CO_2 dissolves into the water; and on longer time-scales chemical reactions incorporate the carbon in minerals. Dissolution trapping is largely determined by convective mixing, which is a rich problem that was first investigated almost 100 years ago. We investigate the influence of convective mixing on dissolution trapping in geological storage of CO_2.

Most formations that can be used for CO_2 storage are slightly tilted. We show with numerical simulations that dissolution trapping must in general be acknowledged when questions about the final migration distance and time of the CO_2 plume are to be answered. The saturations in the plume correspond well to transition zones consistent with capillary equilibrium. The results also show that the capillary transition zone, in which both the supercritical CO_2 plume and the water phase exist and are mobile, participates in the convective mixing. Using linear stability analysis complemented with numerical simulations, we show that the interaction between convective mixing and the capillary transition zone leads to considerably larger dissolution rates and a reduced onset time for enhanced convective mixing compared to when this interaction is neglected. The selection of the wavelength that first becomes unstable remains almost unchanged by the interaction. A statistical investigation of the onset time of enhanced convective mixing under the neglection of the capillary transition zone reveals that it is notably larger than the onset time of instability for three example formations. However, comparison of these simulation results with the investigations in a sloping aquifer preliminarily suggest that the distance that the plume propagates during the onset time of enhanced convective mixing is negligible and that therefore this time can be assumed to be zero, with the possible exception of aquifers that have steep slopes.

Contents

Part I

Background

Chapter 1

Introduction

In this chapter we review the motivation and concept of carbon storage. First, the development of the atmospheric carbon dioxide concentration in the industrial era and its effects are reviewed. This is followed by a description of mitigation strategies. An overview of the physical processes that occur in geological carbon storage and their influence on storage safety is given and the contribution from this thesis is presented.

1.1 Climate change

In 1958, Charles David Keeling initiated his now famous measurements of the carbon dioxide (CO_2) concentration in the atmosphere [50, 51]. Keeling's measurements on Mauna Loa in Hawaii show that the CO_2 concentration has been increasing rapidly since the 1950s. By means of isotope studies of $^{13}CO_2$ [27] and molecular oxygen (O_2) [52, 3], it has been shown that this increase is largely linked to anthropogenic emissions from the burning of fossil fuels. Figure 1.1 displays the CO_2 concentration as obtained by measurements at Mauna Loa compared to data from ice cores. Although there is some natural variability, there has been a 35 % increase in the industrial era [57], leading to a level that is higher than at any previous time during the last 650,000 years [69, 77].

Carbon dioxide together with water vapor and other gases like methane, nitrous oxide and ozone absorb heat radiated from the Earth's surface [57]. An enhanced concentration therefore contributes to global warming, referred to as the greenhouse effect [57]. The most important greenhouse gas apart from water is CO_2 [57]. In past transitions from glacial to interglacial periods that have been investigated, a warming of the climate preceded an enhanced CO_2 concentration [62, 5]. However, feedback from an increased level of greenhouse gases contributed significantly to the transitions [45]. The enhanced CO_2 concentration

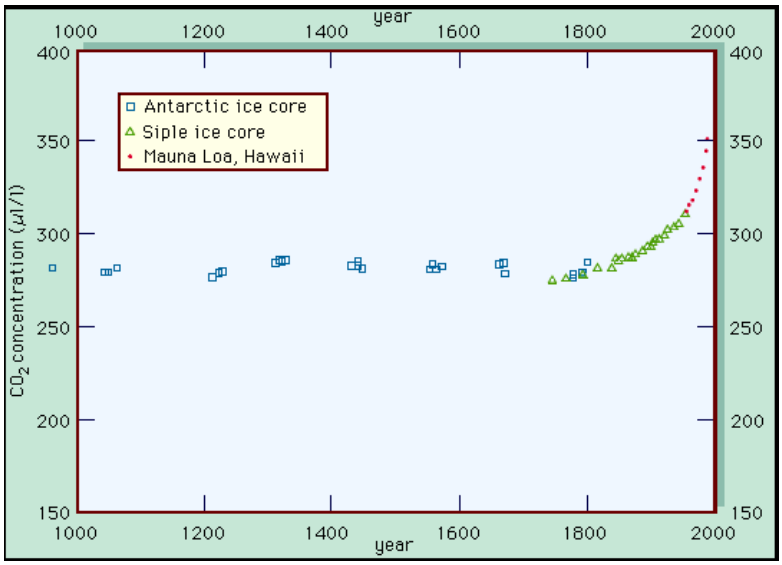

Figure 1.1: Atmospheric concentration of carbon dioxide. Reprinted from http://www.britannica.com/EBchecked/media/69345/Carbon-dioxide-concentrations-in-Earths-atmosphere-plotted-over-the-past, with permission of Encyclopedia Britannica, Inc.

at present greatly exceeds this natural variation and continues to increase. This can cause changes in the climate that have severe impacts on freshwater and food supply, ecosystems and society [44].

Already today, recent climate change has caused changes in natural systems. There is increasing ground instability in permafrost regions, increased runoff in many glacier- and snow-fed rivers, earlier timing of spring events and poleward shifts in ranges in plant and animal species. The oceans have also become slightly more acidic [44]. Estimation of future impacts under the assumption of no mitigation is often performed based on projected changes in precipitation, temperature and sea level [44]. Under these projections, heavy rainfalls and flooding will increase in some regions and at the same time the extent of areas affected by droughts also increase. Later in the century, meltwater from glaciers and snow-cover decrease. Climate change and the rise in sea level lead to coastal erosion and flooding of millions of people towards the end of the century. Continued ocean acidification can lead to enhanced coral mortality, and also in general a reduced biodiversity is expected. The health of millions of people is likely to be affected through for example increased malnutrition and from heat-waves, floods, storms, fires and droughts [44].

Table 1.1: Examples of technologies and associated efforts to achieve one wedge, as presented by Pacala and Socolow [65]. Note that "currently" refers to 2004 when their paper was written.

Option	Effort required to achieve one wedge
Efficient vehicles	Increase fuel economy from 30 miles-per-gallon (mpg) to 60 mpg for 2 billion cars.
Nuclear power	Add twice the currently installed nuclear capacity.
Wind power	Scale up the 2004 installed capacity of wind-generated electricity by a factor 50. This necessitates an area equivalent to 80 % of Norway, some on land and some off-shore. (Multiple land uses are possible.)
Carbon capture and storage	Introduce CCS at coal-fired power plants and other sources corresponding to injection of the current amount used for enhanced oil recovery scaled up by a factor 100.

While all this is very alarming, one should also keep in mind that humans have been able to reverse human-induced trends for global, albeit simpler problems before, regarding for example acid rains and the abundance of chloro-fluoro-carbons that affect the ozone layer [57].

1.2 Mitigation strategies and carbon storage

The largest contribution to the anthropogenic emission of CO_2 (85 %) is the combustion of fossil fuels for energy use [41]. In order to mitigate CO_2 emissions from the energy sector, a variety of actions can be taken, including: use of nuclear and renewable energy sources; use of different energy carriers; combined heat and power; and carbon dioxide capture and storage (CCS) [79]. The effect of different actions on CO_2 mitigation can be illustrated by the use of so-called stabilization wedges, introduced by Pacala and Socolow [65]. A stabilization wedge corresponds to actions that reduce emissions gradually towards 1 Gt carbon per year in the 50 year period following their paper in 2004 [65]. Implementing actions that add up to seven wedges corresponds to stabilized annual emissions during this period, rather than doubled annual emissions which are expected without these special efforts, see Figure 1.2. After this, a decline in emissions is needed if stabilization of atmospheric CO_2 concentration shall be obtained at less than double of the pre-industrial concentration. There is a substantial effort to reach one wedge, some examples are listed in Table 1.1.

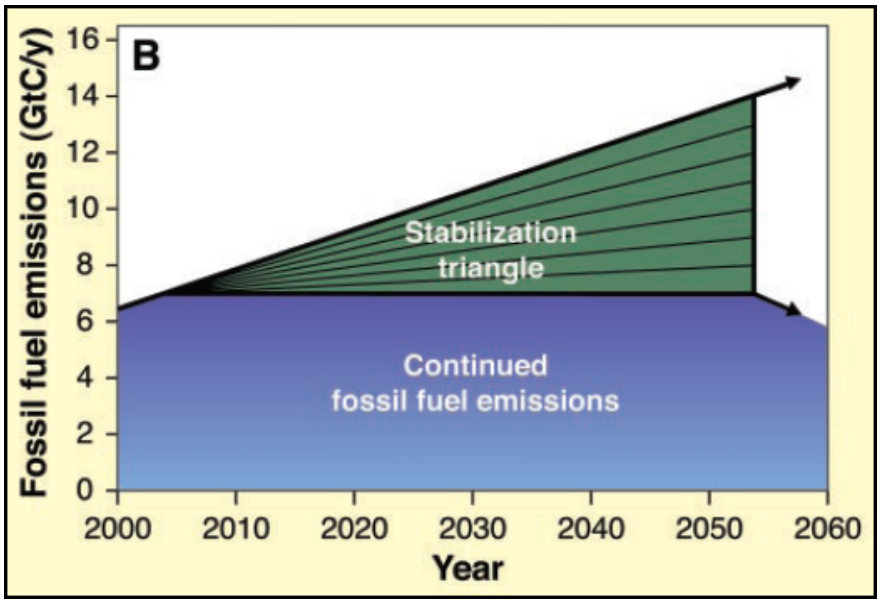

Figure 1.2: Stabilization wedges. From [65]. Reprinted with permission from AAAS.

This thesis treats certain aspects of the fluid dynamics and safety of carbon dioxide capture and storage (CCS). In this technology, CO_2 from predominantly centralized sources like power-plants and large industries is captured and compressed and thereafter transported and stored away from the atmosphere. An overview of CCS is given here. More detailed information can be found in the special report on CCS written by the International Panel of Climate Change, IPCC, and the references therein [43].

There are several options for the capture of CO_2: it can be captured in industrial processes, as well as before and after the combustion of fossil fuels. If pure oxygen is used for combustion, the flue gas contains mostly CO_2 and water. Industrial CO_2 capture has taken place for more than 80 years from purification of natural gas [54]. The separation of CO_2 from other flue gases may involve sorbents, solvents, membranes or distillation. Extensive research is being undertaken to improve the efficiency of these technologies, because capture and separation constitute a large portion of CCS project economy [26].

If the containment system is not in the immediate proximity of the source of CO_2, the CO_2 is transported in pipelines or with ships to the containment system. Pipeline transport requires overpressure protection and leak detection especially in populated areas. Pipelines are already being used for transport of CO_2 from

natural gas sites to sites for enhanced oil recovery. Liquefied CO_2 can be transported in ships in the same way as liquefied natural gas and petroleum gases are transported today.

Storage options include underground geological storage, ocean storage, mineral carbonation and industrial uses. In ocean storage, the deep oceans are considered as storage sites for CO_2. Although the storage potential is large, there have been no large-scale operations of this alternative, primarily because of risk of harming the marine ecosystem [43]. Mineral carbonation is still in the development stage, and industrial use of CO_2 is not expected to contribute much to CO_2 mitigation, because the lifetime of the resulting products is often too short, and the demand for CO_2 is rather small [43].

In contrast to these alternatives, geological storage is an option that is currently in use and that has large potential to contribute to CO_2 mitigation [43]. In geological storage, CO_2 is injected into the pores of sedimentary rocks deep under the land surface or ocean floor. There is ample experience in the techniques from the oil- and gas industry, from current CO_2 storage operations and from storage of acid gas. In addition to being used for for enhanced oil recovery, the CO_2 can be injected into depleted oil- and gas reservoirs, saline formations, unminable coal formations and some other geological media, see Figure 1.3.

The by far largest storage potential is found within saline formations; estimated to at least 1000 $GtCO_2$ and possibly an order of magnitude larger [43]. These are deep sedimentary rocks where the pores are filled with salty water (brine). Saline formations are distributed around the world and are thus in relative proximity of many large sources of CO_2 emissions. The risks associated with geological CO_2 storage projects are related to leakage of CO_2 from the storage formation to other formations where it may pollute potable water, hydrocarbon or mineral resources. Leakage to soils can affect plants and sub-soil animals and leakage into the atmosphere may cause health and safety problems. The expected rates of leakage are in general small but depend on careful site selection. The major challenges of large-scale capture and geological storage are often summarized as: CO_2 capture cost, sequestration safety, legal and regulatory barriers and public acceptance [12]. It is important to consider these challenges in light of the risk of *not* undertaking CO_2 sequestration.

In the remaining part of this thesis we shall focus on storage in saline formations.

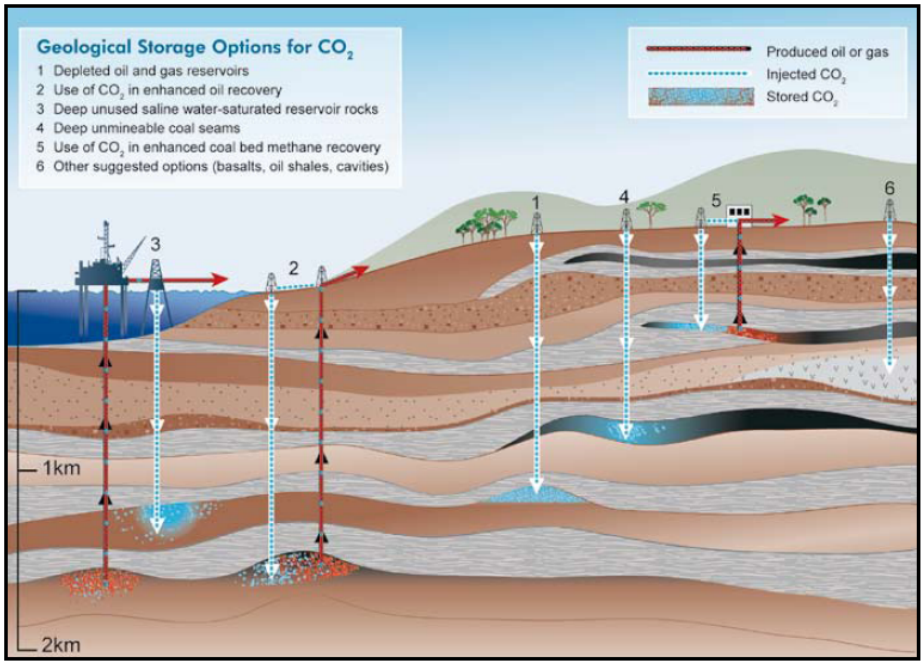

Figure 1.3: Options for storing CO_2 in deep underground geological formations, reprinted with permission from CO2CRC.

1.3 Processes of the injection and post-injection periods

While a detailed description of porous media flow is given in the next chapter, an overview of the transport processes and trapping mechanisms that are important for CO_2 storage in the subsurface are given here.

An understanding of the processes of CO_2 migration in the injection formation is important for the estimation of injectivity, storage capacity and leakage risk. Injection occurs at high pressures to formations that are positioned at least 800 m below the ocean floor or groundwater level. This ensures that CO_2 is in a so-called supercritical state, where it occupies a considerably smaller volume than it would do as a gas at lower pressures [43]. The injection formation must be sealed from above by a rock that fluids cannot easily penetrate, a so-called caprock.

Given that the pores of the injection formation are already filled with brine before the injection of CO_2, the injection process leads to elevated formation pressures. One important aspect of the injection operation is therefore to avoid unwanted fracturing, which could otherwise lead to escape of CO_2 through the

caprock. Careful monitoring is required and also facilitated during the injection period since operations are still in place. Another aspect of the elevated pressures is that the pressure pulse may reach much further than the ultimate transport of CO_2. This pressure "contamination" may interfere with other CCS projects and it may also enhance the risk of pressure driven leakage of CO_2 and brine [12]. In some aquifers it will be necessary to produce brine to reduce the pressures and this generates the question of how to manage the brine after production. For this and other reasons, Court et al. [12] have suggested that water management should be considered as one of the main challenges in geological CCS projects. In the injection operation at InSalah, Algeria, small ground deformation has been noted as an effect of injection, and it has been used to monitor CO_2 movement with satellite imaging [61].

The injected CO_2 is initially mainly transported away from the injection well by the pressure gradients, and upwards because it is lighter than the formation brine. Low-permeability layers within the aquifer, and critically a low-permeability seal above the formation (caprock), therefore control the early flow behavior. Storage in the Utsira formation in the North Sea, for example, has shown that the migration footprint follows the caprock topography (slope) [8]. CO_2 may also be stored in "anticlines" of the low-permeability layers or caprock. This is called stratigraphic trapping.

Injection typically proceeds for a few decades, while the plume may continue to migrate slowly for thousands of years [21]. When injection stops, the pressure gradients will eventually decrease and the main driving force of the plume is its buoyancy. Especially during this post-injection period, brine will replace the trailing edge of the supercritical CO_2 plume [49]. When brine enters pores that were filled by CO_2 it is not able to remove all CO_2, some is left in small pores (see also section 2.3). This is referred to as capillary or residual trapping, and its efficiency increases when more of the aquifer volume is contacted by the plume, i.e. with a larger sweep. Therefore, horizontal low permeable layers within the formation are favorable in this aspect because they restrict the plume from ascending directly towards the caprock. It is also possible to enhance the sweep with engineering methods that reduce the buoyant flow by for example alternating the injection of CO_2 with injection of water. To get a feeling for the storage volumes needed for residual trapping, consider the on-going injection operation into the Utsira formation. The formation extends over an area of approximately 450 km x 75-130 km [30]. When the operation shuts down, some 20 Mt of CO_2 will have been injected [43]. The median of reported porosity values is 38 % [9] and the thickness of the formation is up to 300 m [30]. Using a CO_2 phase density of 700 kg/m^3 and full CO_2 saturation over the entire thickness of the aquifer, the footprint area needed to store this amount as mobile CO_2 is 0.25 km^2. Furthermore, assuming that 20 % of the pore space may be used for residual trapping over the entire thickness,

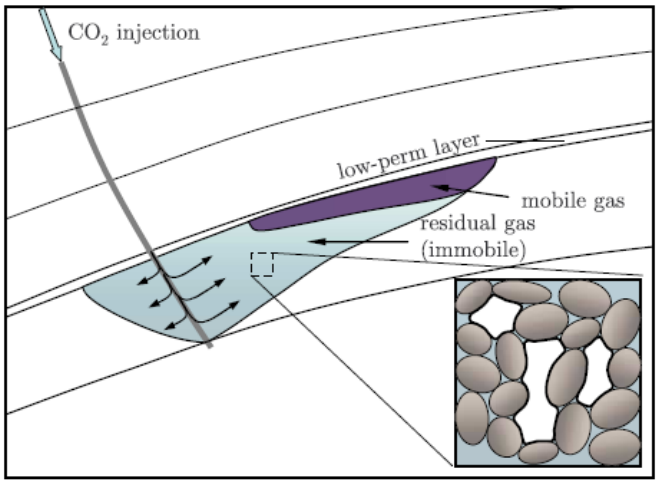

Figure 1.4: Injection, transport and residual trapping of CO_2 in an aquifer. From [49] with permission from the American Geophysical Union.

a foot-print area a factor 5 larger is needed (approximately 1.3 km^2) to store all CO_2 at residual saturation. The full thickness will not be available for residual trapping because CO_2 will tend to migrate preferentially in the upper portions of the aquifer, as discussed above. Already in 2006, seismic imaging showed a plume extent of approximately 2 km^2 (see Figure 1 in [8]). After a long period of storage of CO_2 in the aquifer, the properties of the fluids (wettability, cf. section 2.2) may change [83] and once again the trapped CO_2 may become mobile (if it has not already dissolved at that time).

CO_2 will dissolve from the mobile and residually trapped CO_2 phase into the brine [84]. In the Utsira formation, the solubility of CO_2 is measured at 0.051 $kgCO_2$/kg brine [75] and the brine density is approximately 1000 kg/m^3. With these values an area of 3.4 km^2 is needed to evenly dissolve all CO_2 to the solubility limit if the full aquifer thickness would be used. The full thickness may however not be available to dissolution trapping due to low permeability layers.

The brine density increases around 1 % with dissolved CO_2 content [22] and therefore buoyancy is lost with dissolution and we refer to storage in the brine phase as dissolution trapping. Typically, dense brine with CO_2 will overlay lighter brine without CO_2, causing an unstable setting which may lead to convective mixing [58]. Convective mixing is a major contributor to the dissolution rate [22] because it efficiently provides new fresh brine to regions with high concentration, thereby allowing more CO_2 to dissolve. Over longer periods, the dissolved CO_2 may also react with the formation minerals to produce new minerals that incorpo-

rate the carbon. This is called mineral trapping.

1.4 Contribution of this thesis

This thesis contributes to the understanding of dissolution trapping, and the associated convective mixing, in geological CO_2 storage.

The saline aquifers where CO_2 can be injected are often slightly tilted. There is an up-dip migration of the buoyant CO_2 plume and at the same time, part of the CO_2 is trapped in the water phase by dissolution. Convective mixing is important for dissolution and it acts on a scale much smaller than the large-scale plume migration. This poses difficulties for numerical simulations and hence, attempts to include dissolution by means of up-scaling techniques have been undertaken. There are however uncertainties when a problem that has not been solved is up-scaled. We therefore solve the full problem with direct numerical simulations. The results show that dissolution trapping is a first order trapping mechanism that must in general be acknowledged because it reduces the plume speed and the maximum up-dip extent of the plume. The saturations in the plume correspond well to transition zones consistent with capillary equilibrium and that the two-phase region in the plume (capillary transition zone) participates in the convective mixing.

The influence of the capillary transition zone on convective mixing is studied with linear stability analysis and with direct numerical simulations. The linear stability results show that the capillary transition zone has no significant effect on the selection of the wavelength that first becomes unstable. However, the time until instability begins (the linear onset time) is reduced. Direct numerical simulations for the nonlinear regime show that also the time until enhanced convective mixing begins (the nonlinear onset time) is reduced and that the dissolution rate can be enhanced up to a factor four when the interaction with the capillary transition zone is accounted for. Therefore, the contribution from dissolution to the safety of geological storage of CO_2 begins earlier and can be considerably larger than shown by estimates that neglect the capillary transition zone.

Many investigations have focused on the linear onset time. However, in CO_2 storage, the nonlinear onset time has much larger consequence, since it is not until this time that the instability of the boundary layer leads to enhanced convective mixing. We study the nonlinear onset time including its variations with large ensembles of random initial perturbations. The investigation is performed with direct numerical simulations. Detailed error estimates are given based on the combined effect of discretization, domain size and the finite ensemble size. Enhanced mixing is delayed by a factor 6-8 compared to the linear onset time in the example formations.

Chapter 2

Multiphase, multicomponent porous media flow

This chapter describes the governing features and equations by which the motion of CO_2 and water in a porous medium can be understood and predicted. We shall focus on aspects important for the post-injection period and therefore neglect local thermodynamic inequilibrium and geomechanical responses which are more important during the injection period. The assumption of local thermodynamic equilibrium is comprised of the following: all phases have the same temperature (which may vary in space); there is no other pressure difference between the phases than the capillary pressure (cf. section 2.3); and the phases are in local equilibrium with respect to the exchange of components. In addition, transfer of mass between the rock and fluids (mineralization, adsorption etc) is beyond the scope of this thesis. In the following, boldface symbols represent vectors and matrices and other symbols represent scalars.

2.1 Scale considerations

The behavior and transport of compounds in the subsurface is ultimately determined by their molecular properties. For example, the dipole structure of the water molecule makes water attracted to negatively charged grain surfaces. It is not practically possible however, to study the transport over large volumes based on the molecular scale. Rather, we shall describe the different scales and how we arrive at the so-called macro-scale, which will be our focus. More thorough explanations can be found in e.g. the book of Helmig [33].

First of all, from the molecular scale we wish to transform to a continuum. As an example, in the case of water we now no longer look at the dipole structure and other molecular properties of water but rather on their effects (boiling point

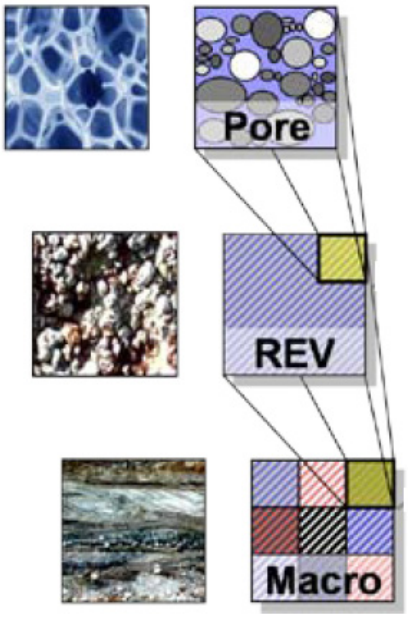

Figure 2.1: The transition from micro- to macro-scale. Printed with permission from Rainer Helmig, Department of Hydromechanics and Modeling of Hydrosystems, University of Stuttgart.

etc) on a continuous phase called water. This consideration of the continuum can be made on different scales; the micro-, macro- and mega-scales. On the micro-scale we treat the phases as continuum but acknowledge the discontinuities between the phases. For the fluids, the flow may then be described by Navier-Stokes equations. This is still a difficult task for porous media flow because of the complex geometries and associated effects. Therefore we most often need to move further, to the macro-scale. At this scale we treat the porous medium and fluids as one continuum with local properties defined by the average over a representative elementary volume (REV) which is localized around the point of interest, see Figure 2.1. It is important to choose the correct size of the REV: it should not be too small so that it is sensitive to variation between the phases; and should not be too large so that it averages over spatial variations that are important for the flow we wish to study. Sometimes it is sufficient to account for spatial variations as parameters of the problem and using larger averaging volumes. This has been referred to as the mega-scale.

2.2 Fundamentals of the macro-scale

CO_2 is injected as a supercritical fluid into the medium where the pores are initially filled with water (brine). After injection there is a competition for the pore space. The volume of pores relative to the total volume of grains and pores in an REV is called the porosity, ϕ. The volume fraction of the pore space in the REV that is occupied by one fluid is called the saturation of that fluid and it is denoted S_α where α denotes the phase. In this competition, the tendency of water to be attracted to the grains is usually larger than the tendency of the supercritical phase to be attracted to the grains. Water is therefore called the wetting phase (denoted by $\alpha = w$) and the supercritical CO_2 phase is called the nonwetting phase ($\alpha = n$). With this notation, we have:

$$S_w + S_n = 1. \tag{2.1}$$

While the wetting phase consists mostly of water and the nonwetting phase consists mostly of CO_2, CO_2 may also dissolve into the wetting phase and water may dissolve into the nonwetting phase. We denote by X_α^C the mass fraction of component C in phase α and therefore:

$$X_w^C + X_n^C = 1, \quad C \in (CO_2, H_2O). \tag{2.2}$$

Under the assumption of local thermodynamic equilibrium, the properties of each phase may be described by a small number of variables, called the state variables. Equations of state describe fundamental thermodynamic relationships between volume, pressure, composition and temperature. We can write it as:

$$\rho_\alpha = \rho_\alpha(p_\alpha, T, X_\alpha^C). \tag{2.3}$$

For CO_2 problems, high accuracy can be obtained by use of relatively simple explicit relations. For example, the Span and Wagner EOS [82] is often used to calculate $\rho_n(p_n, T)$. In Paper C, other explicit relationships often used for densities, solubilities, and viscosities in CO_2 storage applications are referenced.

In simulators developed for the study of oil-gas systems, the cubic Peng-Robinson EOS [68] is often used. Care must be taken if this or other methods of the Redlich-Kwong family of cubic EOS are applied to the system of brine and supercritical CO_2. The reason for this is that the mentioned methods assume that molecules behave the same way in both phases, represented by using equal so-called binary interaction parameters in both phases. This is not a good assumption in the system of brine and supercritical CO_2 because of the polarity of the water molecule.

Under our local thermodynamic equilibrium constraint, phase transitions are not modelled as transport processes but rather as instant equilibrium conditions.

Transport is therefore only modelled as advection and dispersion. Advection is the transport of compounds with the bulk flow of the fluid, described by Darcy's law [28]. Dispersion is the spreading of solutes from the path that would be given by advection. It is due to mechanical dispersion and molecular diffusion [28]. While diffusion is the transport of solute from regions with high mass fractions towards regions with low mass fractions, mechanical dispersion is a more complex phenomena. It is due to velocity differences within pore channels and between pore channels of different size. It is also due to the different inter-connections between pore channels which result in flow paths of different lengths. On the macro-scale we do not resolve these phenomena but rather use a dispersion tensor $\mathbf{D}$ to describe the effect. There is also the possibility of dispersion related to heterogeneities in the medium. This is called macro dispersion. In this case, $\mathbf{D}$ varies with the size of the REV and there is no true REV.

2.3 Multiphase effects

So far we have described the wetting and nonwetting fluid phases. They interact with the solid matrix and with each other. Since the fluids are immiscible (or at least not fully miscible) there is an interface between them, from the viewpoint of the continuous micro-scale. Molecular cohesion within the phases and adhesion between the phases give rise to surface tension [33]. First consider a droplet of wetting phase on a solid matrix which is otherwise covered by nonwetting phase (Figure 2.2*a*). The wetting fluid is the fluid with an acute angle θ between the solid and interface. If the system is in equilibrium the forces acting on the interface are balanced. The surface tension σ_{wn} and angle θ are fixed for given fluid and medium properties. A porous medium can simplistically be described as a bundle of small tubes of different radii (Figure 2.2*b*). At equilibrium the interface has a curvature of radius r which is proportional to the radius of the tube. The pressure will then be largest on the concave (nonwetting phase) side of the interface, and the pressure difference is called the capillary pressure $p_c = p_n - p_w$. It can be calculated by the Laplace equation [33]:

$$p_c = \frac{2\sigma_{wn}\cos\theta}{r}. \tag{2.4}$$

Therefore the capillary pressure is lowest in the tubes of large radius. It means that even small induced pressure differences (capillary entry pressures) can drain (fill with nonwetting phase) the large tubes. For a given distribution of pore sizes, i.e. a given porous medium, and a given induced pressure difference, a certain number of pores will be filled with wetting phase and on the macro-scale this corresponds to a given wetting phase saturation. However, the relation between pressure and

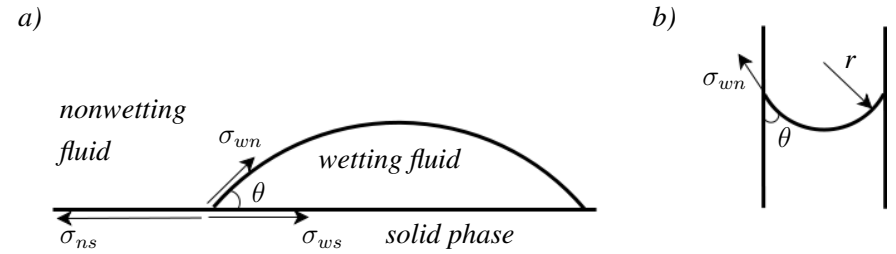

Figure 2.2: *a)* A droplet of wetting fluid. *b)* Wetting fluid below nonwetting fluid in a tube. When surface tension σ_{nw} and other tensions are in balance the interface is stationary.

saturation also depends on if the wetting phase saturation is increasing or decreasing. To understand this hysteresis, we need to improve the approximation of the porous medium. Let the tubes have varying cross sections and consider the case when the wetting fluid flows along the walls of the tubes with nonwetting phase in the tube centres. The varying cross sections lead to varying capillary pressures. Therefore, even if the continuous wetting phase experiences a pressure gradient leading to flow, the pressure gradient in the nonwetting phase can be zero. The wetting phase therefore cannot completely displace the nonwetting phase. The remaining nonwetting phase is trapped as disconnected drops in the pores.

Measurements in a matrix initially filled with wetting fluid and imposing larger and larger pressure differences gives rise to a primary drainage curve, as shown in Figure 2.3*a*, see e.g. [14]. The wetting phase cannot be removed from the smallest pores or crevices no matter the induced pressure (in reasonable time). The corresponding saturation on the macro-scale is called the residual, or immobile, wetting phase saturation, S_{wi}. If the capillary pressure is then reduced from its value at this saturation, the wetting phase imbibes larger and larger pores and the relation between capillary pressure and saturation follows the main imbibition curve. If the process is reversed along this curve, a scanning curve leads to the primary drainage curve and similarly back to the main imbibition curve. The volume fraction trapped nonwetting phase is called the residual nonwetting phase saturation, S_{nr}. The value may be smaller than shown in the figure, if the drainage curve was not completed before imbibition commenced. Residual trapping is important for CO_2 storage.

The relative permeability ($k_{r\alpha}$, Figure 2.3*b*) accounts for the fact that the motion of each fluid is constrained by the co-existence with the other fluid. A larger saturation of a fluid enhances its relative permeability and ability to flow. The relative permeability is zero at the residual saturation of a fluid. The relationship between saturation and relative permeability is also hysteretic.

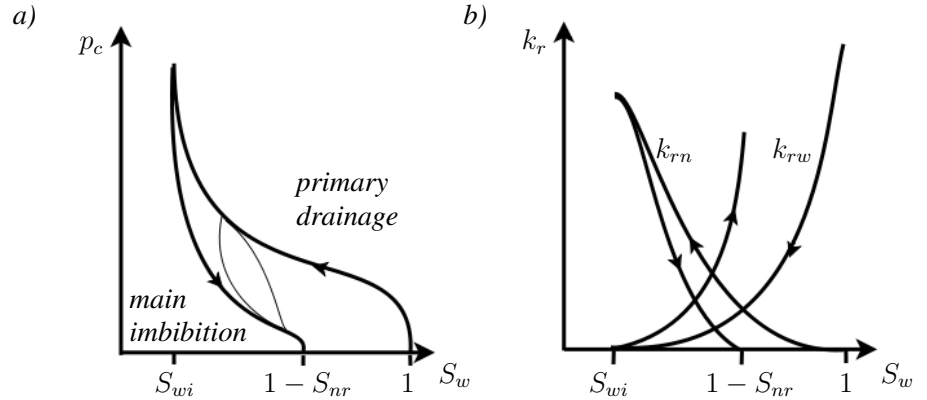

Figure 2.3: *a)* Primary drainage and main imbibition capillary pressure together with scanning curves (thin lines). *b)* Primary drainage and main imbibition relative permeability.

2.4 Darcy's law

We have seen that the relative permeability affects the flow rate in the case of multiphase flow. In this section, an expression for the magnitude of the flow rate is given and we shall begin with single-phase flow. The volumetric flux $\mathbf{u}$ is the volume of a fluid that passes a unit cross-sectional area of porous medium per unit time. It is described by Darcy's law [28]:

$$\mathbf{u} = -\frac{\mathbf{K}\rho g}{\mu} \cdot \nabla h, \tag{2.5}$$

where

$$h = \frac{p}{\rho g} - z \tag{2.6}$$

is the hydraulic head. Here, z is the vertical coordinate increasing downward, $\mathbf{K}$ is the permeability, ρ is the density, g is the size of the gravitational acceleration constant, μ is the viscosity and p is the pressure of the fluid. Darcy's law tells us that fluids in a porous medium flow from large to low pressures and from high to low elevations with a speed that is dictated by the fluid and medium properties. A medium that has large resistance to flow (e.g. small pores) has low permeability. If the resistance to flow varies in different directions, the medium is said to be anisotropic, and the permeability must be described by a symmetric, positive definite tensor. For heterogeneous media the permeability varies as a function of the spatial location. From equation (2.5) we also note that a fluid with large viscosity (like e.g. honey) has a larger resistance to flow compared with a fluid that has low viscosity.

Equations (2.5)-(2.6) may be rewritten as follows if spatial variability in the density is ignored:

$$\mathbf{u} = -\frac{\mathbf{K}}{\mu}(\nabla p - \rho \mathbf{g}). \tag{2.7}$$

Derivations show that this is the more generally applicable relation and that (2.5)-(2.6) involve further assumptions which were fulfilled in Darcy's experiments. Equation (2.7) is valid for Newtonian fluids with relatively small fluxes [11]. In this regime, which is usually applicable to porous media flow, inertia (resistance to change the magnitude or direction of flow), turbulence (randomness in the advection term) and other high-velocity effects can be neglected [11].

When more than one fluid phase is present in the porous medium, a large number of experiments have shown that the flux of each phase α can be described by an extension to Darcy's law [33]:

$$\mathbf{u}_\alpha = -\frac{\mathbf{K} k_{r\alpha}}{\mu_\alpha}(\nabla p_\alpha - \rho_\alpha \mathbf{g}). \tag{2.8}$$

2.5 Mass balance equations

To obtain a solution to the flow of CO_2 and water in the subsurface, Darcy's law and the EOS must be complemented by equations that describe mass conservation of the components as well as initial- and boundary conditions. The mass conservation equations are:

$$\frac{\partial(\sum_\alpha \phi S_\alpha \rho_\alpha X_\alpha^C)}{\partial t} + \nabla \cdot \sum_\alpha (\rho_\alpha X_\alpha^C \mathbf{u}_\alpha - \rho_\alpha \mathbf{D}_\alpha^C \cdot \nabla X_\alpha^C) - Q^C = \quad 0. \tag{2.9}$$

These equations (one equation for each component C) state that the change of mass of a component within the REV, accounting for the presence in both phases, is balanced by advective and dispersive fluxes through the volume boundaries as well as by sources and sinks, Q^C. Note that for truly immiscible flow X_α^C are either 0 or 1 and the equations then describe mass balance of the fluids.

Depending on the state of the system and on the equations of state, the mass balance equations show hyperbolic and/or parabolic characteristics. Hyperbolic conservation laws (in our context) describe transport processes with finite speed. In contrast, parabolic equations describe diffusion processes which in theory have infinite speed, and elliptic equations such as $\nabla^2 p = 0$ describe equilibrium.

A unique solution requires also the formulation of initial and boundary conditions [33]. The initial condition describes the state variables at time zero, for example hydrostatic pressure with small perturbations. The system is connected

with its surroundings through its boundaries. Dirichlet boundary conditions describe the values of state variables at the boundary whereas Neumann conditions describe normal derivatives at the boundary.

Chapter 3

Stability of miscible displacement

3.1 Background

In the previous chapter we discussed the general features of simultaneous transport of CO_2 and water in the subsurface. It is common to focus on either the transport of the two fluids and neglect transport within or between them (immiscible displacement), or to focus on the transport of the CO_2 component within the water phase once it has dissolved and been transported to the single-phase water region (miscible displacement). Both of these settings may encounter instabilities [84, 58]. This means that introduced perturbations grow in time such that the systems progressively depart from the initial states [10]. When the small perturbations grow, a pattern of the saturation (for immiscible displacement) or concentration (miscible displacement) that looks like fingers forms, and the phenomena is therefore called fingering. In this section we shall mainly focus on the instability that occurs when the CO_2 component is transported within the single-phase water region. This instability has a large influence on dissolution trapping. The theory that governs this instability is not unique to CO_2 and water but general for density-driven instability in miscible displacement problems. Here, the density differences can be due to concentration or temperature differences. For example, water density is enhanced with dissolved CO_2 or salt and with reduced temperatures, and the corresponding instability problems have applications to CO_2 storage, flows around salt domes and geothermal energy production. In CO_2 storage, there is also an interplay between immiscible displacement and stability of miscible displacement [20, 80].

Stability problems in viscous fluids (i.e. non porous media) were first studied by Rayleigh [72], in 1916. Horton and Rogers in 1945 [40] and Lapwood

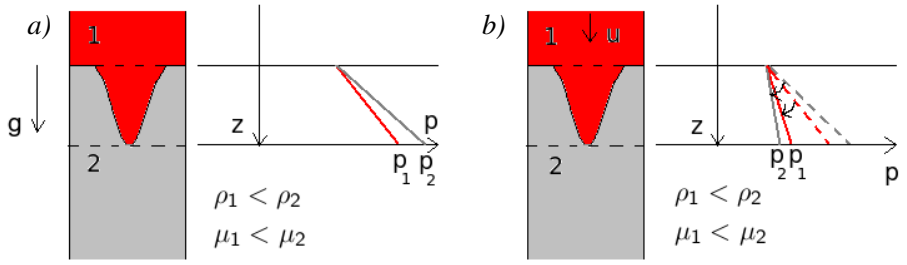

Figure 3.1: Driving forces of viscous fingering displaying *a*) a stable system, and *b*) an unstable system. The lines to the right in each figure show the pressure gradients with the same color coding as the left part of the figures.

in 1948 [56] studied stability in porous media subject to vertical linear temperature gradients and performed the first linear stability analysis of these problems, called Darcy-Bénard problems (or sometimes Rayleigh-Bénard when the porous medium context is not given). The so-called Rayleigh-Taylor problem on the other hand considers two fluids with a sharp interface and no diffusion [18]. There is a large range of problems between these two classical problems, e.g. the Elder problem [16, 17] in which part of the lower boundary is suddenly heated and the base state (i.e. the state without perturbations) evolves in time.

3.2 Forces driving instabilities

We shall here describe the driving forces for viscous and density driven instability, based on the study by Hill in 1952 [38]. Hill considered an idealized porous medium with two fluids separated by a sharp interface with a small perturbation. The fluids were initially at rest and he ignored dispersive mechanisms, such as mechanical dispersion, diffusion or surface tension (the Rayleigh-Taylor problem). Figure 3.1 displays some of the physical insights from his paper. In this example the top (red) fluid is lighter than the fluid beneath. In Figure 3.1*a* the system is initially at rest with a small perturbation. Since there is no capillarity the pressure is continuous over the interface. Due to the reduced density of the upper fluid, the pressure gradient within the perturbation is lower than that of the surrounding fluid. Therefore, the perturbation disappears with time. This setting is stable. In contrast, Figure 3.1*b* displays the same fluids and perturbation when the top fluid is injected with flow rate $\mathbf{u}$ and the flow rate is assumed to be the same in the lower fluid. The associated pressure gradients are lower than static. The pressure gradient decreases most in the lower fluid, which has a higher viscosity. Therefore, the flow is unstable above a critical flow rate, $\mathbf{u}_c$. Dumore [15] used

similar arguments to obtain the critical flow rate. He also included a static transition zone. The critical rate with a sharp interface is obtained when the pressure gradients in both fluids are equal:

$$\mathbf{u} = -\frac{K}{\mu_\alpha}\left(\frac{dp_\alpha}{dz} - \rho_\alpha \mathbf{g}\right), \tag{3.1}$$

$$\frac{dp_\alpha}{dz} = -\frac{\mu_\alpha \mathbf{u}}{K} + \rho_\alpha \mathbf{g}, \tag{3.2}$$

$$\mathbf{u}_c = \frac{\rho_2 - \rho_1}{\mu_2 - \mu_1} K \mathbf{g}. \tag{3.3}$$

We note that there are four combinations of stabilizing and destabilizing effects of gravity and viscosity. In particular, if there is no induced velocity and $\rho_1 > \rho_2$ the system is unstable regardless of the viscosity contrast, although a viscosity contrast may enhance or reduce the strength of the instability once flow has commenced. This is the case we shall focus on hereafter. However, we shall have to include dispersion of the perturbation profile as well as dispersion of the base state, because in our miscible displacement problems there is no static base state [39].

3.3 Problem formulation

From this point we shall talk of instabilities caused by concentration differences and apply a transient base state, which is the instability problem relevant for dissolved CO_2. The theory is equivalent to instabilities driven by temperature differences with exchange of concentration to temperature, molecular to thermal diffusivity and setting porosity equal to 1, cf. [73]. Consider a two-dimensional domain with uniform concentration $c = 0$ of CO_2 in a system initially at rest. Note that $c = X_w^{CO_2}\rho_w$ although subscript w will be dropped in the sequel because we shall study the wetting phase only. At time zero, the concentration at the top boundary is elevated and we assume that the density ρ increases with solute concentration, see Figure 3.2. Apart for the occurrence of density in Darcy's law, density is assumed to be constant (the Boussinesq approximation). The viscosity is here also assumed to be constant. The top boundary represents the interface to the two-phase region. The sudden elevation of concentration and zero initial concentration represents arrival of the plume of supercritical CO_2 to this region. We also introduce small perturbations, e.g. close to the top boundary. The equations

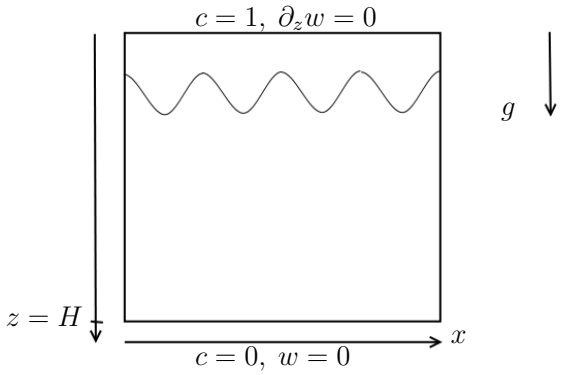

Figure 3.2: Boundary conditions.

that describe this system are:

$$\mathbf{u} = -\frac{K}{\mu}(\nabla p - \rho \mathbf{g}), \tag{3.4}$$

$$\phi\, \partial_t c = -\mathbf{u} \cdot \nabla c + \phi \mathbf{D} \nabla^2 c, \tag{3.5}$$

$$\nabla \cdot \mathbf{u} = 0, \tag{3.6}$$

$$\rho = \rho_0 + \Delta\rho c. \tag{3.7}$$

The initial condition in 2D is $c(x, z, t)$=0 and $\mathbf{u}(x, z, t)$=0, where $\mathbf{u} = (u, w)$, apart from the small perturbations. The boundary conditions are $c(x, 0, t)$=1, $c(x, H, t)$=0 and $w(x, H, t) = 0$, where we may assume a finite domain thickness H or an infinite thickness. The constant concentration at the top boundary condition is motivated by the fast establishment of equilibrium between the phases [22]. The flow condition for the top boundary is yet to be described. A general condition for this boundary assuming a constant effective permeability of the upper layer may be described as a function of the permeability quotient $\mathscr{K} = K_{upper}/K$ [80, 20]. For purely horizontal flux at the top boundary (infinite resistance for water to flow in the two-phase region) we obtain $w(x, 0, t) = 0$ and for zero resistance we obtain $\partial_z w(x, 0, t) = 0$. The former condition has been the most investigated.

Before turning to details of the base state and perturbations, the problem will be rewritten in a non-dimensional formulation. When stability does not depend on the domain thickness it is most natural to use a diffusive length-scale. Then, we scale the problem with the characteristic velocity $u_c = K\Delta\rho g/\mu$, length $l_c = D\phi/u_c$ and time $t_c = D\phi^2/u_c^2$. (We are here assuming isotropic permeability and pure diffusion. The effects of anisotropic permeability and dispersion

will be discussed in section 3.7.) In addition, the pressure is scaled such that the dimensional pressure p is obtained from the non-dimensional pressure P by the relation $p = D\mu\phi/K(P + \rho_0/\Delta\rho\, z)$. The non-dimensional form of the equations is:

$$\mathbf{u} = -(\nabla P - c\mathbf{e_z}), \tag{3.8}$$

$$\partial_t c = -\mathbf{u}\cdot\nabla c + \nabla^2 c, \tag{3.9}$$

$$\nabla\cdot\mathbf{u} = 0. \tag{3.10}$$

When perturbations are small it may be assumed that the modes are normal, i.e. that they do not interact with each other. Therefore, each mode with horizontal wavenumber k may be studied individually as is often done in linear stability theory. Then the concentration, pressure and velocities are rewritten as a sum of base states and perturbation components as shown here for the concentration:

$$c(x,z,t,k) = c_0(z,t) + \hat{c}(z,t,k)\, e^{ikx}, \tag{3.11}$$

where, $\hat{c}(z,t,0) = \hat{w}(z,t,0) = 0$. The finger wavelength is $\lambda = 2\pi/k$. The base state (subindex 0) diffusive transport is described by:

$$c_0(z,t) = 1 - \mathrm{erf}\left(z/(2\sqrt{t})\right), \quad (z > 0) \tag{3.12}$$

$$c_0(0,t) = 1, \tag{3.13}$$

$$u_0(z,t) = w_0(z,t) = 0. \tag{3.14}$$

3.4 Time- and length-scales in the linear regime

Diffusion is initially very strong and therefore any perturbations in the system first decay. After a time called the linear onset time, diffusion has diminished enough that the first mode becomes unstable. At all later times, there will be a range of wavenumbers with positive growth rate between the long-wave cutoff $k = k_L$ and the short-wave cutoff $k = k_S$. The long-wave cutoff (long wavelength) occurs because the driving force is vertical and restricted to the diffusive boundary layer thickness while momentum is lost over long lateral distances. The short-wave cutoff (small wavelength) occurs because diffusion is most severe on perturbations with small wavelengths. There would be no short-wave cutoff without diffusion, and we would also not be able to describe the perturbations on the macro-scale in that case. The dominant wavenumber decreases gradually in time. From the analysis by Riaz et al. [74] it is also apparent that the nominal thickness of the diffusion layer and the dominant wavelength are proportional. The instabilities

prefer an isotropic shape. We also showed in Elenius et al. [20] that the nominal diffusion layer thickness at onset with vertical top boundary flux corresponds well with an isotropic mode, where only the lower half is placed in the diffusive boundary layer and the other half is placed in the two-phase region above.

An understanding of the time- and length-scales is important for practical purposes, such as understanding the possibility of interference with structures in the media, as well as for the performance of accurate numerical and physical experiments. The selection of modes and the linear onset time depend on the properties of the porous medium and fluid. It is often described by means of the Rayleigh number:

$$Ra = \frac{K\Delta\rho g H}{\phi D \mu}. \tag{3.15}$$

The Rayleigh number is the fraction of destabilizing to stabilizing forces. The larger the permeability and density difference, the easier it is for instabilities to grow whereas large values of porosity, diffusion and viscosity will smear out and slow down flow. In Darcy-Bénard problems, the initial solute (or temperature) profile is linear. Convection cells are bounded by the upper and lower boundaries of the domain and only develop for large enough H corresponding to $Ra > 4\pi^2$ for layers that are unbounded in the horizontal direction [76]. On the other hand, for transient base states developing from an initial homogeneous concentration in deep domains, convection cells are bounded by the depth of the diffusion layer only. In this case H does not influence stability and the Rayleigh number is not well defined. As noted above, our non-dimensional equations do not depend on Ra or any other parameter. As a consequence we expect to observe the same phenomena for any Ra, but changes in Ra due to factors other than H would change the dimensional time- and length-scales for the observed phenomena. However, if we were to account for mechanical dispersion, anisotropy, heterogeneity or a finite domain thickness, it would not be possible to remove all parameters from the problem.

Onset times and critical wavenumbers for transient base states have been summarized in a review chapter by Rees [73]. Differences between the reported values are attributed to different definitions of the growth rate, and varying assumptions and placement of the initial perturbations. In Elenius et al. [20], the effect of placement of initial perturbations is discussed in detail.

3.5 Solution strategies for the linear regime

At early times the perturbations are usually very small and the system can be linearized. In this section we shall consider linear stability analysis of miscible

displacement with a transient base state. We will limit the discussion to two spatial dimensions. The analysis is often subdivided into the following steps:

1. Linearize the system and describe it in terms of a base state and perturbation components,

2. Use the coordinate $\xi = z/(2\sqrt{t})$, which is self-similar for the base state concentration profile: $c_0(\xi) = 1 - \mathrm{erf}(\xi)$,

3. Solve the system numerically, or semianalytically with further assumptions.

This methodology was also presented in the review chapter by Rees et al. [73] and we have used it in Elenius et al. [20]. Since the author has not found detailed derivations of step 1 (or 2) in the literature, these are given in Appendix A. The resulting linearized equations in (ξ, t) describe the dynamics of the concentration perturbation $\hat{c}$ and the perturbation in vertical velocity component $\hat{w}$, separately for each horizontal wavenumber k:

$$\left(\frac{1}{4t}\frac{\partial^2}{\partial\xi^2} - k^2\right)\hat{w} = -k^2\hat{c}, \tag{3.16}$$

$$\frac{\partial\hat{c}(t)}{\partial t} - \frac{1}{t}\left(\frac{1}{4}\frac{\partial^2}{\partial\xi^2} + \frac{\xi}{2}\frac{\partial}{\partial\xi} - k^2 t\right)\hat{c} = \sqrt{\frac{1}{\pi t}}e^{-\xi^2}\hat{w}. \tag{3.17}$$

Once these linearized equations are assembled, different strategies can be applied to obtain the growth rate and from this the linear onset time, when the first mode obtains a positive growth rate. The growth rate is exponential and has been defined in several manners, e.g.

$$\sigma(\xi, t, k) = \frac{\partial\hat{c}(\xi, t, k)/\partial t}{\hat{c}(\xi, t, k)}. \tag{3.18}$$

Apart from the linear onset time it is often of interest to obtain the range of modes which have a positive growth rate at later times. From equation (3.18) we note a dependence on ξ. An integral measure can be used, or a certain value based on different arguments. A comparison of results based on different definitions is presented in Elenius et al. [20].

The growth rate can be obtained directly by solving the system numerically. However, finding for example the largest growth rate for all times over all wavenumbers of interest can be a tedious project and semianalytical methods are a desirable alternative. In either case, the profile of the initial disturbance in the streamwise direction is chosen implicitly or explicitly e.g. based on physical insights of the problem at hand or by choosing the most unstable initial profile [20, 80].

One semianalytical method is the dominant mode method, which we have used in Elenius et al. [20]. It assumes that only the streamwise mode exists, which is shown to be dominant in the numerical solution of the initial value problem. The method provides results that show good agreement with the solution of the full linearized problem, especially for small wavenumbers at early times.

In the Quasi Steady State Approximation (QSSA) method, frozen time coefficients are used which means that the growth of the diffusive boundary layer is assumed to be negligible compared with the growth rate of the perturbations. This method can be used for times that are sufficiently large such that the diffusion-effect is not too strong, and sufficiently small such that the linearization is still valid. Riaz et al. [74] showed that with self-similar coordinates, this method gives good results also at early times. Rees [73] showed that the resulting equations differ if the QSSA is applied before or after the coordinate transformation, but information regarding which choice was made in [74] is missing.

In Energy methods, an energy functional $\bar{c} = \left(\int_0^\infty \hat{c}^2 dz\right)^{1/2}$ is defined and the earliest time for which $d\bar{c}/dt = 0$ is obtained with variational methods, see e.g. [6, 73, 80]. Linearization is not undertaken.

In practice, a combination of different methods is often used.

3.6 Fingering in the nonlinear regime

After the linear onset time, there is a period where perturbations grow exponentially. This period ends when the perturbations are so large that the modes begin to interact with each other and we enter the nonlinear regime. After what we shall refer to as the nonlinear onset time, the mass flux through the top boundary will be enhanced compared with the case of purely diffusive redistribution within the domain. With a closed top boundary, mass transfer through the boundary is still diffusive, but convective motion removes water with high concentration from the top, thus enhancing the diffusive flux there. Incropera et al. [42] define convection *heat* transfer as the energy transferred by the combined effect of diffusion and advection, as opposed to transfer by conduction (heat transfer from more energetic to less energetic particles, proportional to the temperature gradient) and radiation (emission of energy from matter by electromagnetic waves). Convective heat transfer occurs between a fluid in motion and a bounding surface when the two are at different temperatures [42]. When convective heat transfer is induced by temperature differences within the fluid, leading to buoyancy forces, it is called natural convection. We shall here use the term convection to also describe *mass* transfer from the combined effect of diffusion and advection. In addition, we note that the motion occurs in closed loops called convection cells within the domain if the boundaries are closed.

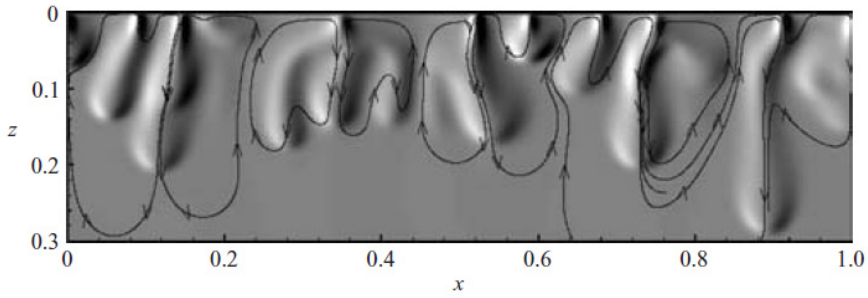

Figure 3.3: Vorticity contours and streamlines from Riaz et al. [74], reprinted with permission from Cambridge University Press. The vorticity is $\omega = -\partial c/\partial x = -\nabla^2\psi$, where ψ is the streamfunction. The vorticity contours overlap with the corresponding concentration contours (not shown here).

The nonlinear onset time depends on the size of initial perturbations and cannot be studied analytically. There is also some sensitivity to the exact shape of the initial perturbations. Therefore it is instructive to perform multiple tests with different initial conditions. If the shapes are varied randomly it is possible to make conclusions about the mean and variation of characteristic parameters, cf. Elenius and Johannsen [19].

The water moves downward in the fingers and upwards between the fingers. When the top boundary is closed, Figures 3.3 and 3.4 show that the fingers form from local feeding sites close to the top boundary. This is due to lateral movement of water towards these feeding sites from both directions. Figure 3.3, when compared to a concentration plot in [74] also shows that the convection cells are closely localized around the visible fingers. The flow structure at the top boundary is different when advective flow is allowed through the boundary, which corresponds to the case when the relative permeability of the water in the two-phase region is above zero, see Figure 3.5. The latter case also gives rise to larger concentration in the fingers and larger mass transfer of solute into the domain.

In the review paper by Homsy [39] it was stated that the evolution of finger shapes may be described by the processes of spreading, shielding and tip splitting. Tip splitting was observed in Hele-Shaw experiments (flow between glass plates, resembling porous media flow) performed by Wooding [87]. In the high-accuracy numerical simulations performed by Riaz et al. [74], a close investigation showed spreading, shielding and merging but no tip splitting. Here, spreading is the lateral growth of fingers due to dispersion. Shielding is when a finger slightly ahead of its neighbor outruns it and shields it from further growth. It occurs because fingers grow in the direction of the pressure gradient, and this gradient is distorted by the first finger.

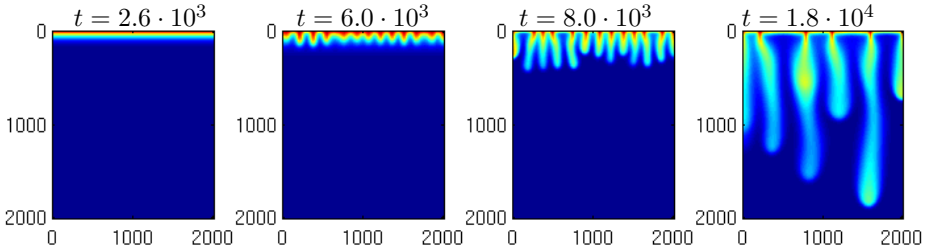

Figure 3.4: Concentration of CO_2 in the domain with horizontal top boundary flux at four non-dimensional times. From Elenius et al. [20]. Red values correspond to high concentrations. At $t = 0$, random fluctuations in the concentration with maximum amplitude 10^{-6} are inserted just below the top boundary. With the given boundary conditions they give rise to non-dimensional velocity fluctuations $u_t \approx 10^{-8}$ at the linear onset time, cf. Figure 3.6.

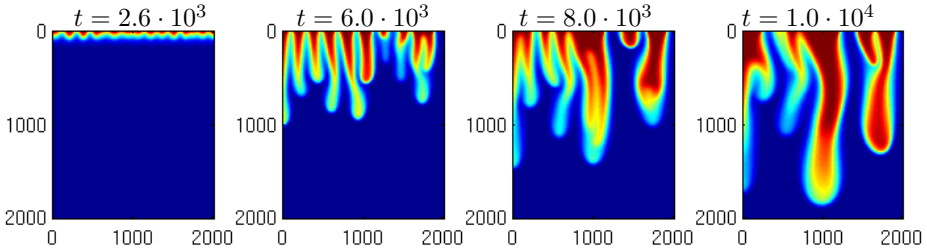

Figure 3.5: Concentration of CO_2 in the domain with vertical top boundary flux and otherwise the same conditions as in the previous figure [20]. Note that the last time shown differs from the previous figure.

Figure 3.6 from Elenius and Johannsen [19] displays the finger velocities and mass transfer rate as a function of time. Note the exponential scale on the vertical axes. It is observed that the fingers obtain an almost constant velocity shortly after the nonlinear onset time, here defined as the time when the dissolution rate reaches a minimum. Note also the large sensitivity of the nonlinear onset time on the size of the initial perturbations.

Hesse [34] showed that the dissolution rate was nearly constant after the nonlinear onset time, with small fluctuations. Figure 3.6 shows that these small fluctuations appear also in the average over a large ensemble. Together with the nonlinear onset time, the magnitude of the dissolution rate can have a large influence on safe geological storage of CO_2. Unfortunately, it is difficult to capture the small scale (about 0.1-10 m [20]) fingers with numerical simulations that govern large-scale CO_2 migration over many kilometers. Therefore different attempts to up-scale convective mixing in CO_2 storage have been undertaken, see e.g. Pruess

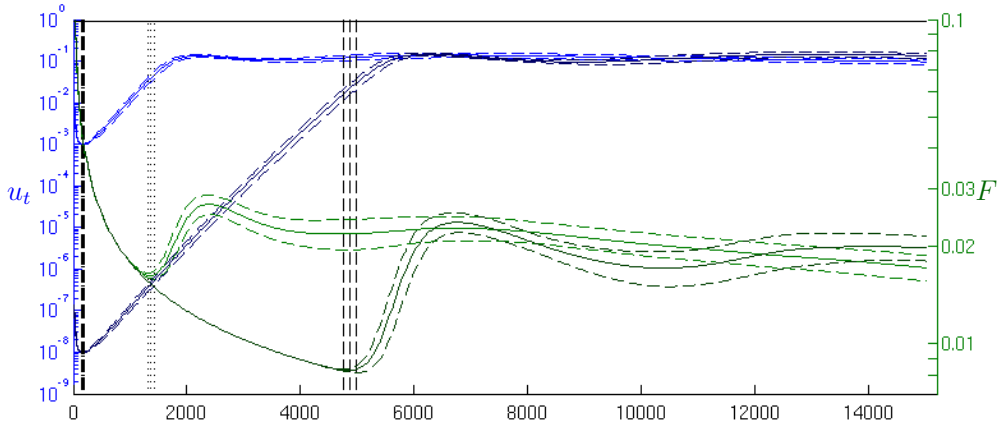

Figure 3.6: Mean values and standard deviations of non-dimensional finger velocity u_t and dissolution rate F, see definitions in Elenius et al. [19]. The lighter blue color corresponds to the lighter green color and it is therefore observed that a larger initial perturbation in the velocities gives rise to earlier nonliner onset. The mean and standard deviation of the linear and nonlinear onset times are shown in dotted lines for the larger initial perturbation and dashed lines for the smaller initial perturbation.

et al. [70], and studies of simpler problems like the ones presented here can provide the necessary input data.

The dissolution rate decreases when the fingers reach the no-flow bottom boundary and this decay rate is larger than in the initial diffusive regime [35] (see also next section).

In the nonlinear regime the flow also becomes increasingly dependent on heterogeneities [29]. Here we have discussed fingering, which occurs in (nearly) homogeneous aquifers. It results in preferential flow paths due to the density differences. If the flow paths are largely affected by heterogeneities and remain also with constant density, the flow is characterized as channeling [85]. According to Waggoner et al. [85], fingering and channeling have fronts that move linearly in time. Deviations from this linear behavior may however occur, due to nonlinear interactions [74, 20]. For very pronounced heterogeneities with small correlation lengths, the flow may become dispersive with a front that propagates as $\sqrt{t}$ also for an unstable density gradient [85, 24].

3.7 Factors controlling convective mixing

Some of the important studies of factors that control or alter stability applicable to miscible CO_2 displacement are presented here and summarized in Table 3.1. We define the linear onset time as the time when perturbations begin to grow and the nonlinear onset time as the time when the dissolution rate becomes enhanced compared with pure diffusion.

Lindeberg and Wessel-Berg [58] calculated stability numbers for typical high permeability aquifers of the North Sea and concluded that density driven convection can occur related to CO_2 storage. Riaz et al. [74] presented linear stability solutions for **homogeneous** aquifers and performed numerical simulations. The linear onset time and the critical-, most dangerous- and cutoff wavelengths as continuous functions of time were obtained.

Ennis-King and Paterson [23] and Xu et al. [88] performed linear stability investigations for **anisotropic** porous media. These were also combined with direct numerical simulations by Ennis-King and Paterson. It was shown that the linear and nonlinear onset times as well as the dissolution rate were affected by anisotropy. Green et al. [29] showed that the dissolution rate in an aquifer with horizontal low-permeability layers of small extent can be modelled approximately based on an anisotropic permeability that uses the effective vertical permeability. However, the onset was found to be determined by the local permeability only. Earlier, Bjørlykke et al. [4] had shown that low-permeability layers may inhibit thermal convection which given typical geothermal gradients require large volumes to develop. Slim and Ramakrishnan [80] provided information about layer thicknesses that are needed for convection, and also for which thicknesses the linear onset time becomes independent of layer thickness. The decay in dissolution rate after interaction with the bottom boundary was described by [35, 31].

Effects of more general **heterogeneous** permeability fields for density-driven convection were studied numerically by Farajzadeh et al. [24]. In most of their simulations and for all three flow regimes - fingering, channeling and dispersive flow -, they found that heterogeneity implied enhanced dissolution rates compared with the homogeneous case.

Convective mixing in the presence of a **capillary transition zone** was studied by e.g. Lu and Lichtner [59], but the influence of the capillary transition zone on stability was not discussed in that paper. In a recent paper by Slim and Ramakrishnan [80], the stability in the linear and nonlinear regime was studied with energy methods, including the effect of capillarity. We have also studied the effect of capillarity in the linear and nonlinear regime [20] including the effect on upscaled parameters in the nonlinear regime. We found that the linear and nonlinear onset times were reduced with this interaction and that the dissolution rate can be greatly enhanced.

Hidalgo and Carrera [37] performed numerical simulations to study the effect of **mechanical dispersion**. The reported nonlinear onset time was reduced by up to two orders of magnitude when dispersion was included in their model problem, although the dissolution rate was not much affected. It is however difficult to draw a firm conclusion about the effect of dispersion on the nonlinear onset time from their paper, because the initial perturbations were introduced by means of numerical errors, and it cannot be excluded that the magnitude of these errors were affected by the changes in the model problem (changed dispersivity). Some authors have stated that dispersion is negligible compared with pure diffusion. For example, Farjazadeh et al. [24] with reference to Bear (1972) state that in their case with Peclet number less than one, the mixing will mainly be determined by molecular diffusion. Also, Slim and Ramakrishnan [80] argue that dispersion can be neglected due to its small calculated size compared with pure diffusion.

Since density-driven instabilities are induced by gravity, the flow has a "simple" rectilinear structure, as opposed to instabilities induced by certain types of forced flow. Therefore, the main areas of study regarding geometry are concerned with wether the full three-dimensional problem is studied or if simplifications are made to a two-dimensional problem, and wether the domain is considered to be finite or infinite ("deep pool") in the vertical direction. Regarding **dimensionality**, Pau et al. [66] showed that for homogeneous media, 3D simulations of convective mixing led to a dissolution rate that was 25 % larger than that estimated by 2D simulations, and to a slightly reduced nonlinear onset time. These changes are small compared with the usual uncertainty of the aquifer permeability. However, the effect of dimensionality may differ for heterogeneous media; and when interaction with the capillary transition zone is considered. In the case of thermal convection, Simmons et al. [78] showed that there was a shift towards larger instability in the 3D case.

Other approximations that are frequently employed especially in analytical treatments are the Boussinesq approximation and the assumption of a linear relation between the aqueous phase density and its CO_2 content. The **Boussinesq** approximation is valid if $Kg\rho l^*/(\mu D) \gg 1$, where l^* is a characteristic length, see [55]. Experimental data from Yang and Gu [89] confirm a **linear relation between concentration and density** for CO_2 storage. It is also common to neglect the effect of **geothermal** gradients on convection of CO_2. Javaheri et al. [46] noted that this effect is negligible in comparison with the effect of concentration gradients, for CO_2 storage.

Special focus on the **dissolution rate** was also attained by Hesse [34] and Pruess and Zhang [71]. Recently, Neufeld et al. [64] presented a new scaling between the mass transfer rate and the Rayleigh number, verified by experiments and numerical simulations. A combination of experimental and numerical work was also performed by Kneafsey and Pruess [53], related to Hele-Shaw cells.

Table 3.1: Features important for convective mixing. "Dissolution rate" refers to the (dimensional) rate after the nonlinear onset time and before influence of the bottom of the aquifer or layer. X denotes that the feature has an important influence, (X) denotes a moderate influence and - denotes an insignificant influence. "Rayleigh number" refers here to the effect of all parameters in the Rayleigh number apart from depth. Note that [29] study the effect of horizontal layers of small lateral extent and that in [66], the effect of dimensionality was studied for homogeneous aquifers with no interaction with the capillary transition zone.

Feature	Linear onset time	Nonlinear onset time	Dissolution rate
Rayleigh number	X [74]	X [19]	X [19]
Initial size of perturbations	- [19]	X [66, 19]	- [66, 19]
Anisotropy	X [88, 23]	X [23]	X [23]
Finite thickness of formation or layer	(X) [80]	?	
Heterogeneity	?	X [29]	X [29, 24]
Interaction with the two-phase regime	X [80, 20]	X [20]	X [20]
Mechanical Dispersion	?	?	-(?) [37]
Dimensionality	?	(X) [66]	(X) [66]

We have studied the time-scales and dissolution rates in the linear and nonlinear regime using statistical measures from multiple realizations [19]. Finally, we note that the dissolution rate can be enhanced in some cases by means of engineering design, see e.g. [32].

Chapter 4

Direct numerical simulations

We have performed direct numerical simulations for the full compositional two-phase problem (2.1, 2.2, 2.8, 2.9), and for the miscible problem (3.8-3.10). We shall here review some common numerical methods for these problems. First recall the mass balance equation given in differential form:

$$\frac{\partial(\sum_\alpha \phi S_\alpha \rho_\alpha X_\alpha^C)}{\partial t} + \nabla \cdot \sum_\alpha (\rho_\alpha X_\alpha^C \mathbf{u}_\alpha - \rho_\alpha \mathbf{D}_\alpha^C \cdot \nabla X_\alpha^C) - Q^C = \quad 0. \quad (4.1)$$

For the discrete solution the variables must be described on a discrete grid and the derivatives in time and space must be discretized. Furthermore, methods must be chosen for the solution of the resulting large system of equations.

4.1 Time discretization and stability

The discrete solution is advanced with time step Δt following an implicit or explicit treatment or a combination of the two. In explicit methods the time-derivatives are obtained as functions of the variables at the old time step only, whilst implicit methods also consider the unknown values of the variables at the new time step. Pressure has an elliptic behavior and therefore its value at any point shows strong dependence on the values at all other points in the domain. For this reason pressure must be treated implicitly. In the fully implicit methods (FIM), all other primary variables are also treated implicitly. For example, in the fully implicit Euler scheme the time-derivative of the full vector of primary variables $\mathbf{x}$ is approximated as:

$$\mathbf{f}(\mathbf{x}^{t+\Delta t}) \approx \frac{\mathbf{x}^{t+\Delta t} - \mathbf{x}^t}{\Delta t}. \quad (4.2)$$

Fully implicit methods are unconditionally stable, i.e. they are stable for any Δt. The time-step size in these methods is instead controlled by the accuracy of the

nonlinear solver. Here, stability has the same interpretation as discussed in the previous chapter, but the interest is on the impact of the time-discretization on perturbation growth rates. Therefore, perturbations are not magnified in time due to the discretization with fully implicit methods, no matter the time-step size. Stability of the numerical scheme is of coarse a very important property for numerical investigations.

The computational cost of large problems can in many cases be reduced if some variables are treated explicitly, which is possible for all variables apart from pressure. The stability of variables treated explicitly is controlled by the CFL (Courant-Friedrichs-Lewy) condition which sets a limit of the time-step size. The condition is that for a hyperbolic partial differential equation (PDE) the domain of dependence of the finite difference scheme must contain the domain of dependence of the PDE [67]. Here the domain of dependence refers to the regions in space-time that have influenced the solution at a given point. The CFL condition is necessary but not always sufficient for stability [67]. It is also possible in the case of hyperbolic and parabolic PDEs to do a Fourier decomposition of the errors and study the growth rate of each mode individually [67].

In the IMPES-formulation (Implicit Pressure Explicit Saturation) all variables apart from pressure are treated explicitly. Sometimes, different time discretization schemes are applied in different parts of the domain depending on the degree of complexity of the flow. This is called AIM, the Adaptive Implicit Method. A larger degree of implicitness is then typically used in regions with high flow rates.

4.2 Space discretization

In numerical simulations, the solution lives on a discrete grid. The space discretization of PDEs is typically done by the finite difference method, FDM, the finite element method, FEM, or the finite volume method, FVM [67]. While the FDM uses the differential form of the equations the FEM and FVM use the integral form which is advantageous for the treatment of Neumann boundary conditions, complex geometries, unstructured grids etc. In the FEM, the variational form is used, see e.g. Aavatsmark [1]. This class of methods allows for flexible gridding and generic discretization but is not locally mass conservative.

We shall focus on the FVM which is most commonly used in commercial reservoir simulators and also used for the simulations performed in this thesis. There are several versions of the method but we shall restrict our attention to the common features here. The FVM conserves mass locally, because the integral form of the equations is applied to each cell Ω_i of the domain Ω. The cells are therefore called control volumes. Integration of (4.1) in each cell with considera-

tion of the divergence theorem leads to:

$$\int_{\Omega_i} \frac{\partial(\sum_\alpha \phi S_\alpha \rho_\alpha X_\alpha^C)}{\partial t} dV + \int_{\partial\Omega_i} \sum_\alpha (\rho_\alpha X_\alpha^C \mathbf{u}_\alpha - \rho_\alpha \mathbf{D}_\alpha^C \cdot \nabla X_\alpha^C) \cdot \mathbf{n}\, dS = \int_{\Omega_i} Q^C dV,$$

where V refers to volume and $\partial\Omega_i$ is the boundary of control volume i. It is divided into several sides $\partial\Omega_{i,j}$. The variables to be integrated in the volume integrals are described at the cell centres and the time-derivatives are discretized according to the previous section. Spatial derivatives are needed to calculate the flux over each side $\partial\Omega_{i,j}$. Consider first horizontal flux $u_{i+1/2}$ between two cells i and $i+1$ as in Figure 4.1*a* and denote the permeability components in the horizontal direction $K_{1,i}$ and $K_{1,i+1}$ in the two cells. (We assume single-phase flow here for simplicity.) Expressions for the flux through the side are first obtained individually from each connected cell, based on the pressures at the cell centres and on the unknown pressure at the side:

$$p_{i+1/2} - p_i = -u_{i+1/2} \frac{\mu_i}{K_{1,i}} (x_{i+1/2} - x_i), \tag{4.3}$$

$$p_{i+1} - p_{i+1/2} = -u_{i+1/2} \frac{\mu_{i+1}}{K_{1,i+1}} (x_{i+1} - x_{i+1/2}). \tag{4.4}$$

Then, by requiring continuity of the flux at the side and adding these two equations, an expression for the flux is obtained:

$$u_{i+1/2} = -\frac{p_{i+1} - p_i}{\frac{\mu_i}{K_{1,i}}(x_{i+1/2} - x_i) + \frac{\mu_{i+1}}{K_{1,i+1}}(x_{i+1} - x_{i+1/2})}. \tag{4.5}$$

For flow with vertical components, the total potential must be used rather than simply the pressure, cf. Figure 4.1*b*. Denote $\psi = p - \rho g z$ where z as before points in the direction of gravity. Then, undertaking similar derivations as in [1], we obtain a generalized expression for the flux:

$$u_{i+1/2} = -\frac{\psi_{i+1} - \psi_i}{\mu_i \frac{\|\mathbf{x}_{i+1/2} - \mathbf{x}_i\|_2}{\|\mathbf{w}_i\|_2} + \mu_{i+1} \frac{\|\mathbf{x}_{i+1} - \mathbf{x}_{i+1/2}\|_2}{\|\mathbf{w}_{i+1}\|_2}}. \tag{4.6}$$

Here, $\mathbf{w} = \mathbf{K}\mathbf{n}$ where $\mathbf{n}$ is the outward pointing normal at the side. We have used the two-point flux approximation (TPFA) which includes only two points in the flux calculation. It is valid if, as in Figure 4.1*b*, the two cell centres and a point on the side can be connected through $\mathbf{w}_i$ and $\mathbf{w}_{i+1}$. This condition must hold for all connections in the domain. If the condition is not fulfilled, a multi-point flux approximation is needed (MPFA).

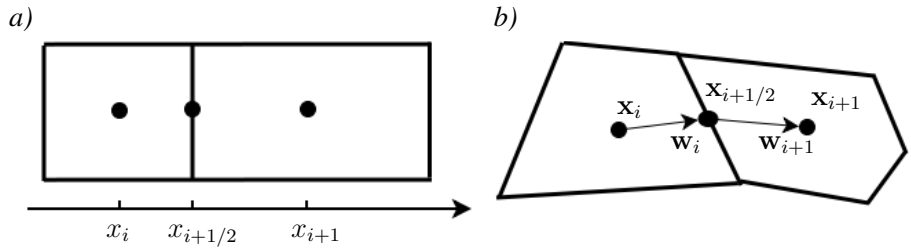

Figure 4.1: Control volumes i and $i+1$ connected by a side $\partial\Omega_{i,j}$. *a)* The flux between the cells is purely horizontal. *b)* The flux has horizontal and vertical components. Parameters needed for the flux calculation are shown. Modified from [1].

The flux is assumed to be constant over each side and integration over the side therefore only involves a multiplication with the side length. The coefficients of the advective flux are often evaluated in the upstream direction (full upwinding) in order to obtain stable solutions. Sometimes, weighted averages are used for pressure dependent variables such as μ and ρ. The upstream cell is the cell with the largest total potential of the two cells considered.

4.3 Consistency, accuracy and convergence

Apart from stability which was discussed above there are three other important general properties of numerical schemes: consistency; accuracy; and convergence. We shall follow [63] and study these concepts for the simple one dimensional diffusion model problem:

$$\frac{\partial c}{\partial t} = \frac{\partial^2 c}{\partial z^2}. \tag{4.7}$$

A simple explicit finite difference scheme with central differences in space is:

$$\frac{C_i^{t+\Delta t} - C_i^t}{\Delta t} = \frac{C_{i+1}^t - 2C_i^t + C_{i-1}^t}{(\Delta z)^2}. \tag{4.8}$$

Here C_i^t is the approximate solution at node i at time t. The equation would no longer hold if we were to insert the true solution c at the nodes. The difference between the left and right hand side is then called the truncation error T:

$$T(z,t) = \frac{c(z,t+\Delta t) - c(z,t)}{\Delta t} - \frac{c(z+\Delta z,t) - 2c(z,t) + c(z-\Delta z,t)}{(\Delta z)^2} \tag{4.9}$$

Now we shall use Taylor expansions around $c(z,t)$, for example:

$$c(z,t+\Delta t) = c(t) + \frac{\partial c}{\partial t}\Delta t + \frac{1}{2!}\frac{\partial^2 c}{\partial t^2}(\Delta t)^2 + \frac{1}{3!}\frac{\partial^3 c}{\partial t^3}(\Delta t)^3 + ... \tag{4.10}$$

to arrive at:

$$T(z,t) = \left(\frac{\partial c}{\partial t} - \frac{\partial^2 c}{\partial z^2}\right) + \left(\frac{1}{2}\frac{\partial^2 c}{\partial t^2}\Delta t - \frac{1}{12}\frac{\partial^4 c}{\partial z^4}(\Delta z)^4\right) + ..., \tag{4.11}$$

$$T(z,t) = \frac{1}{2}\frac{\partial^2 c}{\partial t^2}\Delta t - \frac{1}{12}\frac{\partial^4 c}{\partial z^4}(\Delta z)^2 + ... \tag{4.12}$$

where we have used the fact that c solves (4.7). First of all, note that the truncation error tends to zero as the step sizes in time and space tend to zero regardless of the relation between them, the scheme is unconditionally consistent. If there would be a requirement for this relation the scheme would be said to be conditionally consistent. Any scheme to be used must be consistent.

In our example problem, the highest power of Δt and Δz by which we can say that the truncation error tends to zero is 1 and 2 respectively, cf. equation (4.12). Therefore, the scheme is first order accurate in time and second order accurate in space. A specified accuracy can be obtained with larger step sizes when using a scheme with higher order of accuracy. On the other hand, a higher order scheme in general leads to a more dense matrix which makes each iteration of the linear solver slow down. Also, oscillatory solutions may result from using larger than first order approximations in nonlinear advection terms. As an example, we could not use central differences in [20] with certain boundary conditions.

On a convergent scheme, arbitrarily high accuracy of the solution can be attained by use of a sufficiently fine mesh (if there were no rounding errors). Lax equivalence theorem states that consistency and stability are the necessary and sufficient conditions for convergence of a linear finite difference approximation to a well-posed linear initial-value problem [67].

4.4 Nonlinear solver

In reservoir simulations the nonlinear system of equations is most often solved with Newton-Raphson's method, also called Newton's method. First, the model equations are written in the form:

$$\mathbf{F}(\mathbf{x}^{t+\Delta t}) = \mathbf{0}, \tag{4.13}$$

where we wish to find the solution $\mathbf{x}^{t+\Delta t}$ that fulfills this equation with good accuracy at our new time step. The idea behind Newton's method is to start with an initial guess $\mathbf{x}^{0,t}$, which is usually the solution at the previous time step, calculate

the corresponding value of $\mathbf{F}$, then following its derivative (Jacobian when $\mathbf{x}$ is a vector) to where $\mathbf{F} = \mathbf{0}$. This is the new guess for the solution, $\mathbf{x}^{1,t}$. If the solution is not accurate enough, i.e. $\mathbf{F}(\mathbf{x}^{1,t})$ is too far from $\mathbf{0}$, we proceed as before. If the method has not converged after a certain number of iterations, a smaller time-step size is used. Finally, the converged solution at iteration number N is $\mathbf{x}^{t+\Delta t} = \mathbf{x}^{N,t}$. Formally, the procedure may be written:

$$\mathbf{F}(\mathbf{x}^{n+1,t}) \approx \mathbf{F}(\mathbf{x}^{n,t}) + \frac{\partial \mathbf{F}(\mathbf{x}^{n,t})}{\partial \mathbf{x}} \Delta \mathbf{x}, \tag{4.14}$$

where $\Delta \mathbf{x} = \mathbf{x}^{n+1,t} - \mathbf{x}^{n,t}$. Now for every iteration n this system must be solved, i.e. we wish to find $\mathbf{x}^{n+1,t}$ such that $\mathbf{F}(\mathbf{x}^{n+1,t}) = \mathbf{0}$. The system to solve is:

$$\frac{\partial \mathbf{F}(\mathbf{x}^{n,t})}{\partial \mathbf{x}} \Delta \mathbf{x} = -\mathbf{F}(\mathbf{x}^{n,t}). \tag{4.15}$$

In the next section we shall present different methods to solve this linear equation.

4.5 Linear solvers and preconditioners

The largest computational cost in reservoir simulations is related to the solution of the linear system (4.15). Because the system is very large, direct solvers are not appropriate. Instead, iterative solvers (often preconditioned Krylov methods) are used and therefore several linear iterations are performed in every iteration of Newton's method. An overview of some linear solvers is given here. More detailed descriptions can be found in e.g. [2]. For simplicity let us rewrite (4.15) as:

$$\mathbf{A}\mathbf{x}^* = \mathbf{b} \tag{4.16}$$

where $\mathbf{x}^*$ is the true solution. If we knew $\mathbf{A}^{-1}$ we could directly solve the problem $\mathbf{x}^* = \mathbf{A}^{-1}\mathbf{b}$. Instead, an initial guess by means of a preconditioner $\mathbf{B}$ is established:

$$\mathbf{x} = \mathbf{B}\mathbf{b}. \tag{4.17}$$

The performance of the iterative linear solvers largely depends on the quality of preconditioners, where any iterative solver can be used as a preconditioner for other iterative solvers.

Jacobi's and Gauss-Seidel's methods The perhaps simplest iterative solver is Jacobi's method. First note that:

$$\mathbf{D}\mathbf{x}^* + (\mathbf{L}+\mathbf{U})\mathbf{x}^* = \mathbf{b}, \tag{4.18}$$

$$\mathbf{D}\mathbf{x}^* = \mathbf{b} - (\mathbf{L}+\mathbf{U})\mathbf{x}^*, \tag{4.19}$$

where the matrix $\mathbf{A}$ has been decomposed into its diagonal $\mathbf{D}$, lower triangular $\mathbf{L}$ and upper triangular $\mathbf{U}$ parts. Jacobi's method solves the left hand side for a new estimate of $\mathbf{x}$ using the previous estimate on the right hand side:

$$\mathbf{x}_{m+1} = \mathbf{D}^{-1}(\mathbf{b} - (\mathbf{L}+\mathbf{U})\mathbf{x}_m). \tag{4.20}$$

Iterations proceed until the residual $\mathbf{r} = \mathbf{b} - \mathbf{A}\mathbf{x}$ is small enough. A very similar method is Gauss-Seidel's method, in which the previously computed entries of $\mathbf{x}_{m+1}$ are used for the right hand side as they become available. These methods have slow convergence but can be applied as preconditioners for Krylov methods.

The Conjugate Gradient method The Krylov methods build on orthogonality principles that in some measure minimize the error of every new iteration $m+1$ in the space $\mathbf{x}_0 + S_{m+1}$ where $\mathbf{x}_0$ is the initial guess and S_{m+1} is a Krylov subspace:

$$S_{m+1} = \mathrm{span}(\mathbf{r}_0, \mathbf{A}\mathbf{r}_0, ..., \mathbf{A}^m\mathbf{r}_0), \qquad m \geq 1. \tag{4.21}$$

The oldest and most famous Krylov method is the Conjugate Gradient method (CG). It is efficient for real, symmetric ($\mathbf{A}^T = \mathbf{A}$) systems that are also positive definite ($\mathbf{x}^T\mathbf{A}\mathbf{x} > 0$ for $\mathbf{x} \neq \mathbf{0}$). For every new iteration $m+1$, a search direction vector $\mathbf{d}_{m+1}$ is found such that it is conjugate to all previous search direction vectors. Here conjugate refers to orthogonality with respect to $\mathbf{A}$, i.e. $\mathbf{d}_{m+1}\mathbf{A}\mathbf{d}_l = 0$ for $l < m+1$. The next estimate $\mathbf{x}_{m+1}$ is searched for in the direction of $\mathbf{d}_{m+1}$ with a distance α_{m+1} that minimizes the error along that direction:

$$\mathbf{x}_{m+1} = \mathbf{x}_m + \alpha_{m+1}\mathbf{d}_{m+1}. \tag{4.22}$$

The Generalized Minimum Residual method If $\mathbf{A}$ is not symmetric (as it most often will not be) there are other Krylov methods better suited. An example is the Generalized Minimum Residual (GMRES) method. The iterate $\mathbf{x}_{m+1}$ is found in the subspace $\mathbf{x}_0 + S_{m+1}$ such that the residual is minimized:

$$\min_{\mathbf{x}_{m+1} \in \mathbf{x}_0 + S_{m+1}} \|\mathbf{b} - \mathbf{A}\mathbf{x}_{m+1}\|_2. \tag{4.23}$$

This problem is not solved directly. Instead, vectors in S_{m+1} are written as vectors $\mathbf{q} \in \mathbb{R}^{m+1}$ projected into the subspace by a projector $\mathbf{V}$. We can then write:

$$\mathbf{x}_{m+1} - \mathbf{x}_0 = \mathbf{V}_{m+1}\mathbf{q}_{m+1}. \tag{4.24}$$

The residual is:

$$\mathbf{b} - \mathbf{A}\mathbf{x}_{m+1} = \mathbf{b} - \mathbf{A}\mathbf{x}_0 - \mathbf{A}\mathbf{V}_{m+1}\mathbf{q}_{m+1} = \mathbf{r}_0 - \mathbf{A}\mathbf{V}_{m+1}\mathbf{q}_{m+1}, \tag{4.25}$$

and the least squares problem is rewritten as:

$$\min_{\mathbf{q}_{m+1} \in \mathbb{R}^{m+1}} \|\mathbf{r}_0 - \mathbf{A}\mathbf{V}_{m+1}\mathbf{q}_{m+1}\|_2. \tag{4.26}$$

It is quite inexpensive to find the minimizer $\mathbf{q}_{m+1}$.

Domain decomposition methods In domain decomposition methods, the full problem is decomposed into smaller problems on overlapping (Schwarz methods) or non-overlapping (Substructuring methods) subdomains [81]. The subdomains can be handled independently which is favorable for parallel computing. As an example, in the Schwarz methods a first iterate of the solution is obtained in subdomain 1, the subset of this solution that lies on the boundary of subdomain 2 is used as a boundary condition for the iteration in subdomain 2. This again gives a boundary condition for the next iteration in subdomain 1 and so on.

Multigrid methods are a special case of overlapping domain decomposition methods. The motivation for the development of these methods was to improve the reduction of low-frequency errors, compared to simpler iterative methods. After a few iterations with the basic method, the problem is projected to successive levels of coarser grids and solved there. On the coarse grids a direct solver might be used. Finally, the solution is interpolated back to the original grid where a few more iterations are performed with the basic method.

Choice of method(s) Multigrid methods are well suited for the elliptic (pressure) part of the problem which has a global domain of dependence. For the hyperbolic or parabolic part of the problem (saturation and mass), other methods are better suited. There is a very attractive solver available that treats the elliptic and hyperbolic parts of the problem separately according to their different nature. This is the Constrained Pressure Residual method, CPR [86], which performs well on all kinds of problems but in particular on fully implicit methods.

Chapter 5

Summary of results and outlook

Saline aquifers provide a large potential to store CO_2 for long times, thereby contributing to combat climate change. One of the mechanisms by which CO_2 can become trapped in these aquifers is by dissolution into the brine. This is accompanied by convective mixing. An overview of the relative importance of different storage mechanisms was given in the IPCC Special Report on Carbon Dioxide Capture and Storage [43]. A more detailed understanding of the time and length scales related to the trapping of CO_2 is important for the assessment of potential storage sites. Questions that must be answered are for example: How long will it take until CO_2 is trapped? What is the likelihood that CO_2 reaches regions with faults or leaking wells before it is trapped?

This thesis examines the effect of dissolution trapping. The purpose has been to improve the understanding of the related convective mixing in the linear and nonlinear regimes and its interaction with the mobile plume. The results can also partly be used in directly answering questions such as the above mentioned and are useful as input to models that treat the dissolution implicitly by up-scaling.

5.1 Summary of our results

In this section, we summarize the results and conclusions that the research of this PhD has lead to. The results are presented with a larger level of detail for the investigations of a sloping aquifer than for the other investigations, because the sloping aquifer results have not been presented fully in the corresponding article.

CO_2 trapping in sloping aquifers: High resolution numerical simulations Most saline aquifers are slightly tilted and the buoyant CO_2 plume has a tendency to migrate up-dip. Detailed semi-analytical investigations of the migration of a supercritical CO_2 plume under a sloping caprock were performed by e.g.

Hesse et al. [36] and by MacMinn et al. [60]. Focus was on the long post-injection period and residual trapping was accounted for. Dissolution was disregarded. A similar problem was studied by Pruess et al. [70] with direct numerical simulations. They accounted for dissolution as a sink term. Due to computational limitations, it is very difficult to capture the small-scale convective mixing in the large domains that are needed to study the full development of the plume until it is trapped, and to the knowledge of the author nobody has attempted it before. However, there are uncertainties when up-scaling techniques are applied to a problem that has never been solved. Our purpose in Paper A was therefore to resolve the physics of the full problem to study the importance of dissolution as well as residual trapping in the presence of a capillary transition zone. Simulations were performed using the software GPRS from Stanford University [7, 47]. A finite volume representation was used with cell sizes 3 x 3 m, which is significantly smaller than used in the literature for studies of large-scale plume migration. The fully coupled problem was investigated, apart from dispersion which was not included in the model equations although believed to be more than accounted for by numerical dispersion. The Peng-Robinson EOS was calibrated to give realistic density enhancement with dissolved CO_2 concentration but the solubility was then almost twice as large as would be expected from [13], cf. section 2.2. This leads to an overestimation of the dissolution. Hysteresis in capillary pressure and relative permeabilities was not included, apart from accounting for residual saturations. In order to highlight the fluid dynamics, the aquifer was assumed to be homogeneous with a simple rectangular geometry of length 30 km and thickness 50 m, tilted 1 %. The supercritical CO_2 was placed at the lower end of the aquifer at initialization. Also, because of the very large computational demand, the study was performed in two dimensions. Hydrostatic pressure was applied for the up-dip (right) boundary and all other boundaries were closed. Perturbations leading to fingers arouse from numerical effects.

Compared to simulations with residual trapping only, when dissolution was accounted for, the trapping efficiency was nearly doubled and the speed and maximum up-dip extent of the plume were reduced. The saturations in the plume corresponded well to transition zones consistent with capillary equilibrium. The pressure gradients slightly ahead of the leading tip of the current remained at the initial hydrostatic values, and that opens up the possibility to use a simple moving boundary to model extremely long aquifers.

After writing Paper A we also performed simulations with cells of size 1.6 x 1.6 m. It was too computationally expensive to proceed until the end of plume migration. The mass fraction of CO_2 in the water phase in a 50 x 50 m section of the aquifer is shown in Figure 5.1. We see that the capillary transition zone participates in the convective mixing and that the brine has an undulating movement under the plume due to the combined effect of convective mixing and the

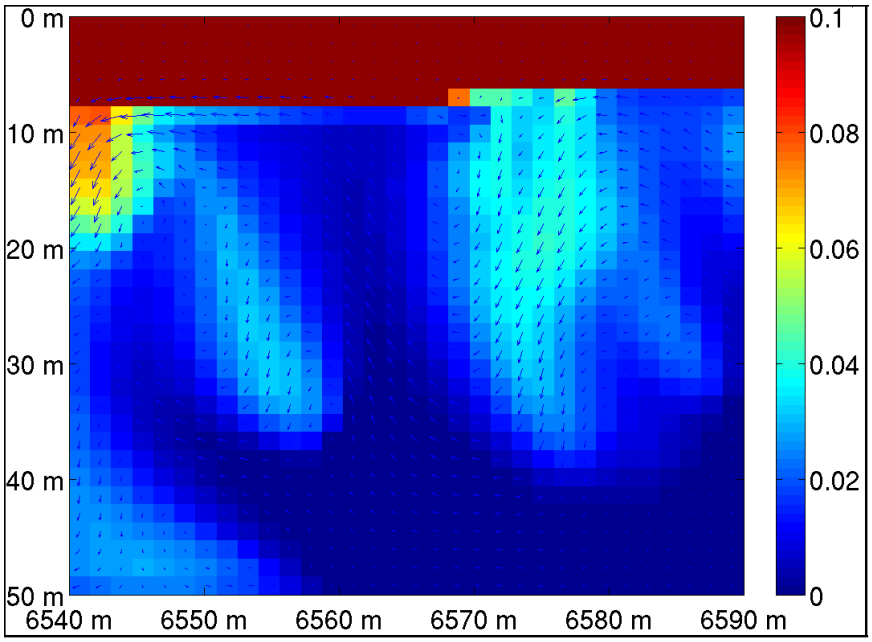

Figure 5.1: Mass fraction of CO_2 in the brine 200 m behind the plume tip. The red color at the top corresponds to the large mass fractions in the two-phase region where also CO_2 phase is present. The CO_2 plume moves to the right in the up-dip direction. The small tilt (1 %) is not shown. Arrows show the direction of brine movement.

down-dip movement to replace the plume.

The effect of dispersion was studied separately in a small domain. Figure 5.2 shows that fingering with the model problem and cell sizes used in the sloping aquifer simulations is weaker than with converged simulations of the full problem including molecular diffusion. We have also seen that there is a delay in the nonlinear onset time with the sloping aquifer case, although the dissolution rates after onset are similar. Therefore, the effect of dissolution is likely underestimated with respect to dispersion. The dissolution-effect is overestimated with respect to the solubility limit but dissolution trapping is thought to be important also with a solubility limit that is a factor two smaller.

Effects of a capillary transition zone on the stability of a diffusive boundary layer In our next paper we investigated the influence of the capillary transition zone on convective mixing. Traditionally, the interface to the two-phase region has been modeled as a no-flow top boundary in detailed finger-

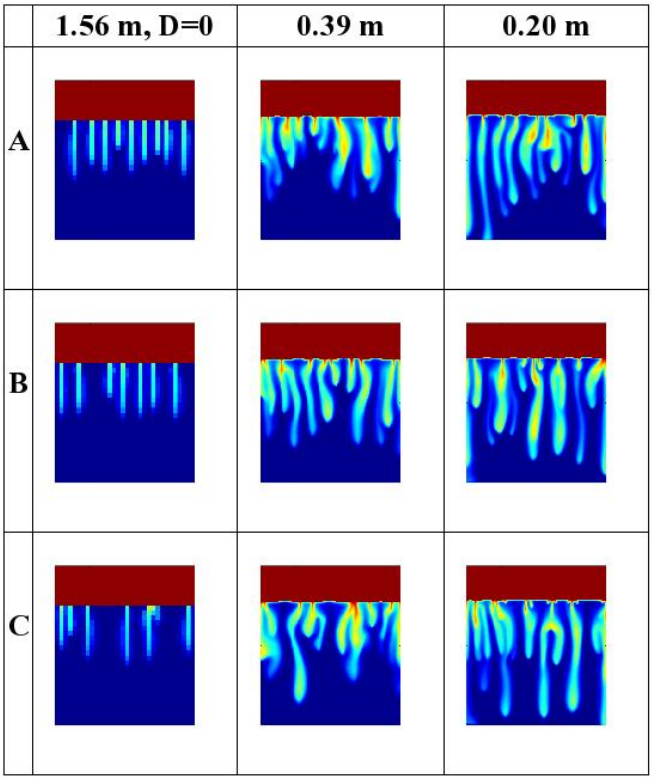

Figure 5.2: Mass fraction of CO_2 in the brine in a small domain 40 years after initialization with saturations consistent with capillary equilibrium at the upper part. Three different initial random perturbations (A, B and C) of the mass fractions were used. The case $D = 0$ corresponds to the performed simulations in the large domain with no dispersion in the model problem and cell sizes 1.56 x 1.56 m, whereas molecular diffusion in the other two cases is included in the model problem ($D = 1 \cdot 10^{-9}$ m^2/s) and the overall fingering behavior is (almost) converged with respect to numerical dispersion.

ing investigations. Our idea was that the convective flux that we had observed in the lower parts of the transition zone could make the system more unstable and increase the mixing compared to what investigations with no-flow boundary had shown.

The early period with transition from stable to unstable modes was studied by means of linear stability analysis. We assumed constant permeability for the brine region and constant effective permeability for the brine in the transition zone. We then gave an expression for the interface conditions and also translated this condition to the dominant mode method. After this, we showed results for the full linearized problem and the dominant mode solution that apply for the end-point of infinite permeability in the transition zone. This corresponds to vertical velocities at the interface rather than horizontal velocities as traditionally used. We found that the influence of the capillary transition zone had no significant effect on the selection of the critical mode. However, the linear onset time was reduced by a factor five, corresponding to instability at thinner diffusive boundary layers.

The nonlinear regime, which cannot be studied with stability analysis, was investigated by means of direct numerical simulations. We used the software d^3f [25, 48] from Gesellschaft für Anlagen- und Reaktorsicherheit (GRS). The results show that the dissolution rate can be enhanced up to four times when the interaction with the capillary transition zone is accounted for, and that also the nonlinear onset time is reduced. This is related to advective inflow of CO_2 saturated water across the interface. Therefore, the contribution from dissolution to the safety of geological storage of CO_2 begins earlier and can be considerably larger than shown by estimates that neglect the capillary transition zone.

Comparison to a paper by Slim and Ramakrishnan [80] show that the method of choosing the initial perturbations has a large influence on the results. Our method using a variable that is self-similar for the diffusion corresponds to insertion of initial perturbations close to the interface. In [80], the most unstable initial perturbation was chosen and it was not restricted to the interface. While the latter choice leads to faster onset times, perturbations localized at the interface will for many physical settings be a better approximation.

On the time scale of non-linear instability in miscible displacement porous media flow Many investigations have focused on the linear onset time. However, in CO_2 storage, the nonlinear onset time has much larger consequence, since it is not until this time that the instability of the boundary layer leads to enhanced convective mixing. In Paper C, the focus is primarily on the identification of the nonlinear onset time. Direct numerical simulations with the simulator d^3f were performed of the miscible displacement problem in a two-dimensional domain with boundaries that were closed to flow. Perturbations were

initiated adjacent to the top boundary. Then the three regimes of the dynamics were identified, namely the development of the stable diffusive boundary layer, the onset and growth of instabilities (linear regime) and the fully non-linear dynamics. The results are generic in the sense that there are no parameters in the non-dimensional model problem. Large ensembles were studied and detailed error estimates are given based on the combined effect of discretization errors in time and space, domain size and the finite sample size. The nonlinear time scales show a dependence on the size of initial perturbations. We estimated this size for three formations that are used for CO_2 sequestration, based on their variations in porosity, and found that the onset of enhanced convective mixing was delayed by a factor 6-8 compared with the linear onset time.

5.2 Outlook

This section begins with a claim and a statement of five hypotheses about the importance of dissolution in CO_2 storage. After this, suggestions to further work are proposed.

Claim

- The effect of trapping mechanisms must be evaluated both with respect to their effect on the distance a plume travels before it is trapped, and with respect to the effect they have on the time it takes until the plume reaches that distance.
  The distance travelled tells us if the plume reaches zones with for example fractures or abandoned wells by which it can escape. A given amount of CO_2 that returns to the atmosphere is likely to have less impact on the environment if it is spread over long times. In hundreds or thousands of years from today, unforeseeable changes in the environment might change the perspective from an elevated atmospheric CO_2 concentration to other issues.

Hypotheses

1. Dissolution is an important trapping mechanism in at least all sloping aquifers with slope ≤ 1 % and available aquifer thickness ≥ 50 m, unless injection occurs directly into a stratigraphic trap where all CO_2 is trapped.
   In Paper A we concluded that dissolution trapping is important in comparison with residual trapping under the conditions of slope and aquifer thickness mentioned here, and with respect to both migration distance and time.

The permeability is usually the parameter with largest variation between aquifers. Neglecting diffusion, a change in permeability can be thought of as a scaling of the time, which applies equally to residual- and dissolution trapping. Under this assumption, the relative impact from these mechanisms on the time for plume entrapment does not change with the permeability and also the final migration distance is unchanged by altered permeabilities. Dissolution trapping is also generally assumed to be important relative to mineral trapping. The relative importance of dissolution over residual trapping might decrease with increased slope and also when the depth available for dissolution is reduced by e.g. lateral low-permability layers within the aquifer. If injection on the other hand occurs directly into a tight stratigraphic trap, all trapping mechanisms apart from stratigraphic trapping may be disregarded.

2. The distance that the plume propagates during the nonlinear onset time is negligible and therefore the nonlinear onset time can be assumed to be zero, with the possible exception of aquifers with slope considerably larger than 1 %.
   In Paper A, the plume speed in an aquifer with permeability 100 mD and slope 1 % was approximately 1 m/year. Using a permeability a factor 5 larger, as for the Tubåen formation, would give a plume speed of approximately 5 m/year, assuming the same slope and CO_2 phase relative permeability. In Paper C we estimated the nonlinear onset time for the Tubåen formation to be 2 months. With a speed of 5 m/year, the plume would then migrate a distance of less than 1 m during the nonlinear onset time. This distance is very small compared to e.g. a total plume migration of several kilometers, and neglecting dissolution over this small distance will most likely not influence the effect of dissolution trapping. The non-dimensional nonlinear onset times vary within a factor 2 in the example formations studied in Paper C, and this variation would not alter the conclusion. Different permeabilities would not change the migration distance given above because both the (dimensional) nonlinear onset time and the plume speed are proportional to the permeability. The magnitude of the relative permeability affects the plume speed but is not thought to vary enough to change this conclusion. A considerably larger slope could perhaps change the conclusion however.

3. When the caprock has a homogeneous tilt, the most important factor for the total dissolution rate G (mass CO_2 dissolved per unit time in the aquifer) is the speed at which the footprint area of the plume is increased.
   The dissolution rate G in Paper A was nearly constant at 1000 kg/year

despite the fact that the areal extent of the plume increased over time. The brine becomes saturated with CO_2 at some distance behind the tip. The value of the maximum dissolution intensity F (mass CO_2 dissolved per unit footprint area and time) has been frequently studied but will not affect G, other than through its effect on the plume speed, see Figure 5.3.

4. Dissolution trapping is most efficient in aquifers that have irregular caprock topography or where the plume is transported partly in fractures within the aquifer. Under these conditions there is a stronger dependence of the dissolution rate G on the maximum dissolution intensity F than described in hypothesis 3.
   Hypothesis 3 was based on the assumption that only the water beneath the plume is used for dissolution. On the other hand, under the conditions described here, the plume propagates heterogeneously in the horizontal (lateral) direction and therefore more surrounding water can be used. If this leads to a state where the water does not become saturated under the plume, the dissolution intensity can be maintained at the value F (or at least above zero) which corresponds to an influence of F on G.

5. *a)* Horizontal low-permeability layers can shield brine deep in the aquifer from dissolution, thereby reducing the impact of dissolution trapping.
   b) In addition, these layers may impede the development of convection cells especially in aquifers with low permeability, because the wavelengths of importance may not fit between the layers.
   a) A reduced water volume will permit less CO_2 to dissolve per footprint area of the plume.
   b) As a first approximation we use stability theory developed under the assumption of infinite aquifer thickness. Then from Figure 4 in Paper B it is seen that wavelengths considerably shorter than the critical wavelength do not become unstable at any time. Therefore, the critical wavelength must fit between the structures for convection to occur. The critical wavelength for the Krechba formation is 10 m under the same assumption and the most unstable wavelength grows in time.

Further work Related to the results and conclusions presented, and considering the hypotheses stated above, the following further investigations are proposed:

- The interaction between the plume and fingering deserves more attention, especially since it was shown in Paper A to have significant influence on both plume speed and final migration distance. It would be very good to have one benchmark solution to the full problem that is converged with

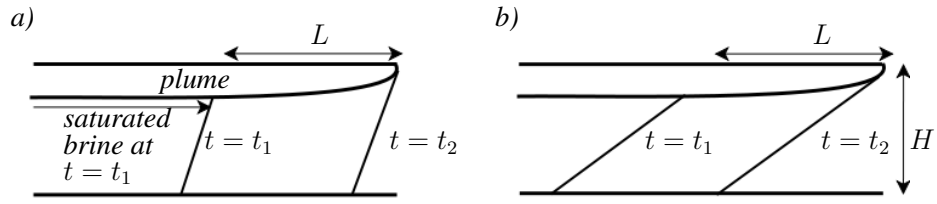

Figure 5.3: *a)* A plume of supercritical CO_2 advances under the caprock (to the right in the figure). Beneath the plume, CO_2 dissolves into the brine and the brine eventually becomes saturated. Here, this is shown at times t_1 and t_2 as a concentration which is either zero or at the solubility limit. The mass of CO_2 that dissolves between these times in a cross-section of width W is the concentration at the solubility limit multiplied by the volume, $V = L\ H\ W$. *b)* In this case, the maximum dissolution intensity is smaller, but the same amount of CO_2 dissolves between times t_1 and t_2 since the volume has not changed. This assumes that L is the same, i.e. that the plume speed is not affected by the dissolution intensity.

respect to discretization errors. Simplified models could then be compared to this solution. Simpler expressions for the solubilities than used in Paper A should be used to facilitate comparison. A numerical method must be developed for this particular problem to speed up simulations. For example, a moving boundary can be used and possibly equilibrium of the CO_2 phase can be assumed in the direction perpendicular to the slope.

- More attention should be given to the isolated effect of the capillary transition zone. The factor 4 larger dissolution rate that we found as an upper end-point of the influence of the capillary transition zone should be determined in more detail.

- The effect of low-permeability structures on dissolution trapping needs more attention than it has been given in the literature so far.

Bibliography

[1] I. Aavatsmark. Bevarelsesmetoder for elliptiske differensialligninger. *University of Bergen, Lecture notes*, 2007.

[2] R. Barret, M. Berry, T.F. Chan, J. Demmel, J.M. Donato, J. Dongarra, V. Eijkhout, R. Pozo, C. Romine, and H. Van der Vorst. *Templates for the solution of linear systems: Building blocks for iterative methods, 2nd edition*. SIAM, 1994.

[3] M. Bender, T. Ellis, P. Tans, R. Francey, and D. Lowe. Variability in the O-2/N-2 ratio of southern hemisphere air, 1991-1994: Implications for the carbon cycle. *Global Biogeochem Cycles*, 1:9–21, 1996.

[4] K. Bjørlykke. *Petroleum geoscience: From sedimentary environments to rock physics*. Springer, 2010.

[5] N. Caillon, J.P. Severinghaus, J. Jouzel, J-M. Barnola, J. Kang, and V.Y. Lipenkov. Timing of atmospheric CO_2 and antarctic temperature changes across Termination III. *Science*, 299:17281731, 2003.

[6] J-P. Caltagirone. Stability of a saturated porous layer subject to a sudden rise in surface temperature: Comparison between the linear and energy methods. *Q. J. Mech. appl. Math.*, 33:47–58, 1980.

[7] H. Cao. Development of techniques for general purpose simulators. *PhD Stanford University, USA*, 2002.

[8] R.A. Chadwick, D. Noy, R. Arts, and O. Eiken. Latest time-lapse seismic data from Sleipner yield new insights into CO_2 plume development. *Energy Procedia*, 1:2103–2110, 2009.

[9] R.A. Chadwick, P. Zweigel, U. Gregersen, G.A. Kirby, S. Holloway, and P.N. Johannessen. Geological reservoir characterization of a CO_2 storage site: The Utsira Sand, Sleipner, northern North Sea. *Energy*, 29:1371–1381, 2004.

[10] S. Chandrasekhar. *Hydrodynamic and hydromagnetic stability*. Oxford University Press, 1961.

[11] Z. Chen, G. Huan, and Y. Ma. *Computational methods for multiphase flows in porous media*. Society for Industrial and Applied Mathematics, 2006.

[12] B. Court, M.A. Celia, J.M. Nordbotten, and T.R. Elliot. Active and integrated management of water resources throughout CO_2 capture and sequestration operations. *Submitted to GHGT-10*.

[13] Z. Duan and R. Sun. An improved model calculating CO_2 solubility in pure water and aqueous NaCl solutions from 273 to 533 K and from 0 to 2000 bar. *Chem. Geol.*, 193:257271, 2003.

[14] F.A.L. Dullien. *Porous media: Fluid transport and pore structure*. Academic Press, 1992.

[15] J.M. Dumore. Stability considerations in downward miscible displacement. *SPE Journal*, 231:356–362, 1964.

[16] J.W. Elder. Steady free convection in a porous medium heated from below. *J. Fluid Mech.*, 27:29 – 48, 1967.

[17] J.W. Elder. Transient convection in a porous medium. *J. Fluid Mech.*, 27(3):609–623, 1967.

[18] J.W. Elder. The unstable thermal interface. *J. Fluid Mech.*, 32:69–96, 1968.

[19] M.T. Elenius and K. Johannsen. On the time scales of non-linear instability in miscible displacement porous media flow. Submitted to Computational Geosciences.

[20] M.T. Elenius, J.M. Nordbotten, and H. Kalisch. Effects of a capillary transition zone on the stability of a diffusive boundary layer. Submitted to IMA J. Appl. Math.

[21] M.T. Elenius, H.A. Tchelepi, and K. Johannsen. CO_2 trapping in sloping aquifers: High resolution numerical simulations. *XVIII International Conference on Water Resources*, 2010.

[22] J.P. Ennis-King and L. Paterson. Role of convective mixing in the long-term storage of carbon dioxide in deep saline formations. *SPE*, 84344, 2003.

[23] J.P. Ennis-King and L. Paterson. Role of convective mixing in the long-term storage of carbon dioxide in deep saline formations. *SPE J*, 10(3):349–356, 2005.

[24] R. Farjazadeh, P. Ranganathan, P.L.J. Zitha, and J. Bruining. The effect of heterogeneity on the character of density-driven natural convection of CO_2 overlying a brine layer. *Adv. Water. Resour.*, 34:327–339, 2011.

[25] E. Fein. d^3f-Ein Programmpaket zur Modellierung von Dichtestrmungen. *GRS, Braunschweig, GRS-139*, 1998.

[26] J.D. Figueroa, T. Fout, S. Plasynski, H. McIlvried, and R.D. Srivastava. Advances in CO_2 capture technology. The U.S. Department of Energys Carbon Sequestration Program. *International J. of Greenhous Gas Control*, 2:9–20, 2008.

[27] R.J. Francey and G.D. Farquhar. An explanation of C-13/C-12 variations in tree rings. *Nature*, 297:28–31, 1982.

[28] R.A. Freeze and J.A. Cherry. *Groundwater*. Prentice Hall, 1979.

[29] C. Green, J. Ennis-King, and K. Pruess. Effect of vertical heterogeneity on long-term migration of CO_2 in saline formations. *Energy Procedia*, 1:1823–1830, 2009.

[30] U. Gregersen and P.N. Johannessen. Distribution of the Neogene Utsira Sand and the succeeding deposits in the Viking Graben area, North Sea. *Marine and Petroleum Geology*, 24:591–606, 2007.

[31] H. Hassanzadeh, M. Pooladi-Darvish, and D. Keith. Scaling behavior of convective mixing, with application to CO_2 geological storage. *AIChE Journal*, 53(5):1121–1131, 2007.

[32] H. Hassanzadeh, M. Pooladi-Darvish, and D.W. Keith. Accelerating CO_2 dissolution in saline aquifers for geological storage - mechanistic and sensitivity studies. *Energy and Fuels*, 23:3328–3336, 2009.

[33] R. Helmig. *Multiphase flow and transport processes in the subsurface*. Springer, 1997.

[34] M.A. Hesse. Mathematical modeling and multiscale simulation for CO_2 storage in saline aquifers. *PhD Stanford University, USA*, 2008.

[35] M.A. Hesse, A. Riaz, and H.A. Tchelepi. Resolving density fingering during CO_2 sequestration: A challenge for reservoir simulation. *Proceedings, CO2SC symposium, Lawrence Berkley National Laboratory, March 20-22*, 208-211, 2006.

[36] Hesse, M.A. and Orr, F.M.Jr. and Tchelepi, H.A. Gravity currents with residual trapping. *J. Fluid Mech.*, 611:35–60, 2008.

[37] J.J. Hidalgo and J. Carrera. Effect of dispersion on the onset of convection during CO_2 sequestration. *J. Fluid Mech.*, 640:441–452, 2009.

[38] S Hill. Channeling in packed columns. *Chem. Eng. Sci.*, 1(6):247–253, 1952.

[39] G.M. Homsy. Viscous fingering in porous media. *Ann. Rev. Fluid Mech.*, 19:271–311, 1987.

[40] C.W. Horton and F.T. Rogers. Convective currents in a porous medium. *J. Appl. Phys.*, 16:367370, 1945.

[41] IEA. Building the cost curves for the industrial sources of non-CO_2 greenhouse gases. *Greenhouse Gas R&D Programme*, PH4/25:www.iea.org, 2003.

[42] F.P. Incropera, D.P. DeWitt, T.L. Bergman, and A.S. Lavine. *Fundamentals of heat and mass transfer, 6th ed.* Wiley, 2007.

[43] IPCC. *IPCC Special Report on Carbon Dioxide Capture and Storage. Prepared by Working Group III of the Intergovernmental Panel on Climate Change [Metz, B., O. Davidson, H. C. de Coninck, M. Loos, and L. A. Meyer (eds.)].* Cambridge University Press, 2005.

[44] IPCC. *Summary for Policymakers. In: Climate Change 2007: Impacts, Adaptation and Vulnerability. Contribution of Working Group II to the Fourth Assessment Report of the Intergovernmental Panel on Climate Change, M.L. Parry, O.F. Canziani, J.P. Palutikof, P.J. van der Linden and C.E. Hanson (eds.).* Cambridge University Press, 2007.

[45] E. Jansen, J. Overpeck, K.R. Briffa, J.-C. Duplessy, F. Joos, V. Masson-Delmotte, D. Olago, B. Otto-Bliesner, W.R. Peltier, S. Rahmstorf, R. Ramesh, D. Raynaud, D. Rind, O. Solomina, R. Villalba, and D. Zhang. *Palaeoclimate. In: Climate Change 2007: The physical science basis. Contribution of Working Group I to the Fourth Assessment Report*. Cambridge University Press, 2007.

[46] M. Javaheri, J. Abedi, and H. Hassanzadeh. Linear stability analysis of double-diffusive convection in porous media, with application to geological storage of CO_2. *Transp. Porous Med.*, 84:441456, 2010.

[47] Y. Jiang. Techniques for modeling complex reservoirs and advanced wells. *PhD Stanford University, USA*, 2007.

[48] K. Johannsen. Numerische aspekte dichtegetriebener strömung in porösen medien. *Professorial dissertation (habilitation), Heidelberg, Germany*, 2004.

[49] Juanes, R. and E.J. Spiteri and F.M. Orr Jr and M.J. Blunt. Impact of relative permeability hysteresis on geological CO_2 storage. *Water Resources Research*, 42(W12418):doi:10.1029/2005WR004806, 2006.

[50] C.D. Keeling. The concentration and isotopic abundances of carbon dioxide in rural and marine air. *Geochim. Cosmochim. Acta*, 24:277–298, 1961.

[51] C.D. Keeling. Rewards and penalties of monitoring the Earth. *Annu. Rev. Energy Environ.*, 23:25–82, 1998.

[52] R.F. Keeling and S.R. Shertz. Seasonal and interannual variations in atmospheric oxygen and implications for the global carbon-cycle. *Nature*, 358:723–727, 1992.

[53] T.J. Kneafsey and K. Pruess. Laboratory flow experiments for visualizing carbon dioxide-induced, density-driven brine convection. *Transp. Porous Med.*, 82:123–139, 2010.

[54] A.O. Kohl and R.B. Nielsen. Gas purification. *Gulf Publishing Co., Houston, TX, USA*, 1997.

[55] A.J. Landman and R.J. Schotting. Heat and brine transport in porous media: the Oberbeck-Boussiesq approximation revisited. *Transp Porous Med.*, 70:355–373, 2007.

[56] E.R. Lapwood. Convection of fluid in a porous medium. *Proc. Camb. Philos. Soc.*, 44:508521, 1948.

[57] H. Le Treut, R. Somerville, U. Cubasch, Y. Ding, C. Mauritzen, A. Mokssit, T. Peterson, and M. Prather. *Historical overview of climate change. In: Climate Change 2007: The physical science basis. Contribution of Working Group I to the Fourth Assessment Report*. Cambridge University Press, 2007.

[58] E. Lindeberg and D. Wessel-Berg. Vertical convection in an aquifer column under a gas cap of CO_2. *Energy Convers. Mgmt*, 38:229–234, 1997.

[59] C. Lu and P.C. Lichtner. High resolution numerical investigation on the effect of convective instability on long term CO_2 storage in saline aquifers. *Journal of Physics*, Conference Series 78:012042, 2007.

[60] MacMinn, C.W. and M. L. Szulczewski and R. Juanes. CO_2 migration in saline aquifers. Part 1: Capillary trapping under slope and groundwater flow. *J. Fluid Mech.*, 662:329–351, 2010.

[61] A. Mathieson, I. Wright, D. Roberts, and P. Ringrose. Satellite imaging to monitor CO_2 movement at Krechba, Algeria. *Energy Procedia*, 1:2201–2209, 2009.

[62] E. Monnin, A. Indermühle, A. Dällenbach, J. Flückiger, B. Stauffer, T.F. Stocker, D. Raynaud, and J-M. Barnola. Atmospheric CO_2 concentrations over the last glacial termination. *Science*, 291(5501):112114, 2001.

[63] K.W. Morton and D.F. Mayers. *Numerical solution of partial differential equations*. Cambridge University Press, 2005.

[64] J.A. Neufeld, M.A. Hesse, A. Riaz, M.A. Hallworth, H.A. Tchelepi, and H.E. Huppert. Convective dissolution of carbon dioxide in saline aquifers. *Geophysical Res. Letters*, 37:L22404, 2010.

[65] S. Pacala and R. Socolow. Stabilization wedges: Solving the climate problem for the next 50 years with current technologies. *Science*, 305:968–972, 2004.

[66] G.S.H. Pau, J.B. Bell, K. Pruess, A.S. Almgren, M.J. Lijewski, and K. Zhang. High-resolution simulation and characterization of density-driven flow in CO_2 storage in saline aquifers. *Adv Water Resour*, 33:443–455, 2010.

[67] J. Peiró and S. Sherwin. *Finite different, finite element and finite volume methods for partial differential equations. In: S. Yip (ed.) Handbook of Materials Modeling. Volume I: Methods and Models*. Springer, 2005.

[68] D-Y. Peng and D.B. Robinson. A new two-constant equation of state. *Ind. Eng. Chem. Fundam.*, 15:1, 1976.

[69] J.R. Petit, J. Jouzel, D. Raynaud, N.I. Barkov, J.M. Barnola, I. Basile, M. Bender, J. Chappellaz, M. Davisk, G. Delaygue, M. Delmotte, V. M. Kotlyakov, M. Legrand, V. Y. Lipenkov, C. Lorius, L. Pépin, C. Ritz, E. Saltzmank, and M. Stievenard. Climate and atmospheric history of the past 420,000 years from the Vostok ice core, Antarctica. *Nature*, 399:429436, 1999.

[70] K. Pruess, J. Nordbotten, and K. Zhang. Numerical simulation studies of the long-term evolution of a CO_2 plume under a sloping caprock. *Proceedings, TOUGH symposium, September*, 2009.

[71] K. Pruess and K. Zhang. Numerical modeling studies of the dissolution-diffusion-convection process during CO_2 storage in saline aquifers. *Technical Report LBNL-1243E, Lawrence Berkley National Laboratory, USA*, 2008.

[72] Lord Rayleigh. *Phil. Mag. (6th ser.)*, 6:529–546, 1916.

[73] D.A.S. Rees. *The instability of unsteady boundary layers in porous media, In P. Vadász (ed.), Emerging topics in heat and mass transfer in porous media*. Springer Science+Business media B.V., 2008.

[74] A. Riaz, M. Hesse, H.A. Tchelepi, and F.M. Orr. Onset of convection in a gravitationally unstable diffusive boundary layer in porous media. *J. Fluid Mech.*, 548:87–111, 2006.

[75] C.A. Rochelle and Y.A. Moore. The solubility of supercritical CO_2 into pure water and synthetic Utsira porewater. *British Geological Survey*, CR/02/052, 2006.

[76] A. Selim and D.A.S. Rees. The stability of a developing thermal front in a porous medium. I Linear theory. *Journal of Porous Media*, 10(1):1–15, 2007.

[77] U. Siegenthaler, T.F. Stocker, E. Monnin, D. Lüthi, J. Schwander, B. Stauffer, D. Raynaud, J-M. Barnola, H. Fischer, V. Masson-Delmotte, and J. Jouzel. Stable carbon cycle-climate relationship during the late Pleistocene. *Science*, 310(5752):13131317, 2005.

[78] C.T. Simmons, V. Kuznetsov, and D.A. Nield. Effect of strong heterogeneity on the onset of convection in a porous medium: Importance of spatial dimensionality and geologic controls. *Water Resources Research*, 46:W09539, 2010.

[79] R.E.H. Sims, R.N. Schock, A. Adegbululgbe, J. Fenhann, I. Konstantinaviciute, W. Moomaw, H.B. Nimir, B. Schlamadinger, J. Torres-Martnez, C. Turner, Y. Uchiyama, S.J.V. Vuori, N. Wamukonya, and X. Zhang. *Energy supply. In Climate Change 2007: Mitigation. Contribution of Working Group III to the Fourth Assessment Report of the Intergovernmental Panel on Climate Change [B. Metz, O.R. Davidson, P.R. Bosch, R. Dave, L.A. Meyer*

(eds)], Cambridge University Press, Cambridge, United Kingdom and New York, NY, USA. Cambridge University Press, 2007.

[80] A.C. Slim and T.S. Ramakrishnan. Onset and cessation of time-dependent, dissolution-driven convection in porous media. *Phys. Fluids*, 22:124103, 2010.

[81] B. Smith, P. Bjørstad, and W. Gropp. *Domain Decomposition*. Cambridge University Press, 1996.

[82] R. Span and W.A. Wagner. A new equation of state for carbon dioxide covering the fluid region from the triple-point temperature to 1100 k at pressure up to 800 mpa. *J. Phys. Chem. Ref. Data*, 26:1509–1596, 1996.

[83] F. Tewes and F. Boury. Formation and rheological properties of the supercritical CO_2-water pure interface. *J. Phys. Chem.*, 548:892–898, 2005.

[84] L.G.H. van der Meer. Investigations regarding the storage of carbon dioxide in aquifers in the Netherlands. *Energy Convers. Mgmt*, 33(5-8):611–618, 1992.

[85] J.R. Waggoner, J.L. Castillo, and L.W. Lake. Simulation of EOR processes in stochastically generated permeable media. *SPE Formation Evaluation*, pages 173–180 (June), 1992.

[86] J.R. Wallis, R.P. Kendall, and T.E. Little. Constrained residual acceleration of conjugate residual methods. *SPE*, 13563, 1985.

[87] R.A. Wooding. Growth of fingers at an unstable diffusing interface in a porous medium or Hele-Shaw cell. *J. Fluid Mech.*, 39(3):477–495, 1969.

[88] X. Xu, S. Chen, and D. Zhang. Convective stability analysis of the long-term storage of carbon dioxide in deep saline aquifers. *Adv Water Resour*, 29:397–407, 2006.

[89] C. Yang and Y. Gu. Accelerated mass transfer of CO_2 in reservoir brine due to density-driven natural convection at high pressures and elevated temperatures. *Ind. Eng. Chem. Res.*, 45:2430–6, 2006.